ONE GEV BEAM ACCELERATION IN A ONE METER LONG PLASMA CELL

A Proposal to the
Stanford Linear Accelerator Center

Primary Investigators:

R. Assmann, C. Joshi, T. Katsouleas, W. Leemans, R. Siemann

Collaboration:

S. Chattopadhay, W. Leemans, LBNL

R. Assmann, P. Chen, F.J. Decker, R. Iverson, P. Raimondi, T. Raubenheimer, S. Rokni, R.H. Siemann, D. Walz, D. Whittum, SLAC

C. Clayton, C. Joshi, K. Marsh, W. Mori, G. Wang UCLA

T. Katsouleas, S. Lee, USC

April 1997

Abstract

A plasma-based wakefield acceleration (PWFA) experiment is proposed that will accelerate parts of an SLC bunch by up to 1 GeV/m over a length of 1 m. A single SLC bunch is used to both induce wakefields in the one meter long plasma and to witness the resulting beam acceleration. The proposed experiment will explore and further develop the techniques that are needed to apply high-gradient plasma wakefield acceleration to large scale accelerators. The one meter length of the experiment is about two orders of magnitude larger than other high gradient PWFA experiments and the 1 GeV/m accelerating gradient is roughly ten times larger than that achieved with conventional metallic structures. Using existing SLAC facilities, the proposed experiment will allow the study of high gradient acceleration at the forefront of advanced accelerator research.

Table of Contents

I. Introduction

The energies of most interest for high energy physics today have reached the multi-TeV level. Linear colliders offer the only possibility to access this energy regime with e+e- collisions. Practical limitations on the size and the cost of linear colliders can only be overcome if the acceleration per unit length is significantly increased. While there are attempts to push the gradients in conventional metallic structures to 1 GeV/m, plasma-based acceleration concepts have attracted considerable interest. By replacing the metallic walls of conventional structures with "plasma-walls" many limitations are avoided and very high gradients can be achieved. A recent laser-driven plasma wakefield acceleration (PWFA) experiment has measured an accelerating gradient of 100 GeV/m[1].

Although plasma-based experiments have shown impressive advances in their accelerating gradients, they are quite short, extending over only a few mm. This proposal aims at demonstrating high gradient acceleration in a 1 m long plasma cell. Plasma modules of this length would be well suited for building a future linear collider. The intended use of the existing SLAC linac for the proposed experiment limits the achievable gradient to about 1 GeV/m. Though not as high as achieved by other plasma-based experiments, this gradient is much larger than in any metallic structure. It would be the first time that plasma-based structures accelerate particles by one GeV.

The basic idea for the proposed experiment is to use a single SLC bunch to both excite the plasma wakefield (head of the bunch) and to witness the resulting acceleration (tail of the bunch). For many reasons, the SLC beam is the ideal driver for a plasma acceleration test. It has high energy; it is very stiff and is not subject to distortion or depletion over the length of the experimental section proposed here. In addition, neither the driving particles nor the accelerated particles will significantly phase slip over the length of the experimental section. All of these factors suggest the possibility for a clean test of plasma wakefield acceleration and the opportunity to make detailed comparisons to theoretical models.

The experiments proposed here will assess the viability of wakefield transformers based on beam-driven plasmas. The plasma wakes excited by particle beam and laser drivers are quite

similar (although there are slight differences and these will be discussed in Sec. II). However, the physics of beam propagation (self-focusing, stability, optimal profile shapes, etc.) are quite different. Moreover, particle beam and laser drivers have different scalings for energy gain per stage and efficiency, which may make particle drivers more attractive at ultra-high energies. By designing flexibility into the plasma source and/or drive bunch length, we will be able to explore some of the most important phenomena. Specifically, we can measure the transformer ratio (i.e. the decelerating and accelerating fields within the bunch), transverse focusing fields, and the dependence of the gradient on plasma density, bunch length, beam and plasma radius. Furthermore, increasing the plasma density or bunch length will enable a first test for electron hose instability[2]. A secondary benefit of the proposed experiment will be the opportunity to explore the new physics and technology issues associated with particle beam rather than laser drivers.

We propose to place a meter-long plasma of appropriate density in the path of the SLC beam at IP-1 of the FFTB[3,4]. The PWFA experiment will replace the E144[5] (nonlinear Compton scattering) experimental setup. The beam parameters needed for the proposed experiment are routinely achieved during standard SLC operation. Most important are a beam intensity of between 3.5 to 4×10^{10} electrons and a suitable bunch length (σ_z = 0.6 mm) and shape. It will be shown that the high current longitudinal bunch profiles in the SLC linac are well suited. Normalized emittances and transverse beam jitter are not critical and can be significantly larger than the standard SLC values at 46.6 GeV.

In order to minimize the impact and cost of the proposed experiment we plan for parasitic running at 10 Hz during PEPII[6] operation. PEPII will already accelerate the linac beams to 30 GeV for positron production. We avoid additional costs for the maintenance and operation of the RF in the last third of the linac by only requiring 2-3 sectors of acceleration downstream of the positron extraction point. The additional acceleration is needed in order to maintain efficient BNS damping and a small final energy spread. The beam energy in the FFTB will be 30 GeV. Minor modifications in the dumpline transport will allow safe operation of the FFTB with a high current 30 GeV beam. Though planning for 30 GeV, it is important to note that the PWFA experiment can always be carried out at 46.6 GeV, if appropriate.

The development of the different parts of the experiment is well under way. The proposed plasma cell has been built at UCLA and is presently being tested. The beam-induced plasma wakefields have been modeled at USC. The transport of the SLC beam into the FFTB, through the plasma cell and into the beam dump has been studied carefully at SLAC. Finally, the appropriate beam diagnostic has been specified based on the extensive experience at SLAC and LBNL. We believe that all critical components needed for a successful experiment are in place.

The proposed experiments are envisioned to take place in stages. The first stage will simply place a meter-long plasma of appropriate density in the path of the SLC beam near the end of the FFTB. We expect the head of the bunch to be decelerated by about 0.2 GeV while tail particles are accelerated by up to 1 GeV. The resulting change in energy distribution, will be detected by a time-resolved energy measurement with a streak camera. The wakefield will be diagnosed in detail by subtracting the energy distribution signals with and without the plasma. The second set of experiments proposed here will vary the plasma density, plasma length, and/or beam bunch length to test scaling laws for wake amplitudes and electron hose instability.

We can envision a rich physics program of follow-on experiments not proposed here. Some of these include tests of beam shaping to demonstrate the possibility of high transformer ratios[7], the use of a separate witness beam with a variable delay to fully probe the wakefields[8], the guiding of laser beams with the SLC beam in a plasma over hundreds of Rayleigh lengths[9] and the outcoupling of the plasma wakes as a unique high-power 100 GHz source[10]. We also note that the peak accelerating gradient in the experiment is expected to increase from 1 GeV/m to 2.5 GeV/m if the SLC RMS bunch length can be reduced from 0.6 mm to 0.4 mm. The successful completion of the experiments proposed here will undoubtedly provide a major impetus to advanced accelerator research as well as contribute to fundamental understanding of plasma and beam physics.

The remainder of this proposal is organized as follows: In Sec II we review the theory and scaling laws for plasma wakefield acceleration and apply these to the design of a 1 GeV experiment at SLAC. In Sec. III, IV and V the three major components of the experiment are described in detail: Beam Delivery, Plasma Source, and Diagnostics. A timetable for the experiment is presented in Sec. VI.

II. Wakefield Theory and Design Criteria[11-17]

As illustrated in Figure 1, the basic concept of the plasma wakefield accelerator is to use a high-current drive-beam to excite a large plasma wake that can accelerate trailing particles. The wake is created when the space charge of the drive beam displaces plasma electrons in much the same way that a boat creates an ocean wake by displacing water. In this case the plasma ions provide the restoring force on the displaced electrons and the wake phase velocity is at the beam velocity (≈ c). This creates a high-gradient accelerating structure with a wavelength set by the plasma density $\left[\lambda_p \approx 1\text{mm} \cdot (10^{15}\ \text{cm}^{-3}/n_o)^{1/2}\right]$.

In this section we summarize the design equations and scaling laws for wakefield excitation in plasmas. First, we review 2-D linear theory (Part A). Although this is strictly valid only for the case when the beam is much less dense than the plasma ($n_b << n_o$), an assumption not valid for our experiment, the linear scaling laws are a useful guide. Our experiment could be modified to test the linear theory simply by expanding the beam spot size. However, for nominal spot sizes less than one hundred microns, the experiment will operate well into the non-linear or blowout regime (Part B). This regime is predicted to have several advantages for preserving beam quality of the accelerated electrons (Ref. 20). Analytic tractability is not one of the advantages of this regime, however, and we rely on numerical solutions of the fluid equations to develop operating design criteria for the experiments proposed here. In Part C we will model the final designs in detail with 2-1/2 D particle-in cell (PIC) simulations. The focusing force from the plasma and its effect on the beam is considered in Part D.

A. Linear Theory

The linear wakefield response of a plasma to a short particle beam pulse or a short laser pulse is quite similar. To show the similarities and differences we present here a unified derivation of the plasma wakefield response to either a laser or particle beam pulse. Later we will drop the laser term and specialize to the particle case of interest for the experiment proposed here. The linear response of a cold uniform plasma to a short pulse of electrons or photons can be obtained easily by substituting the momentum equation for plasma electrons

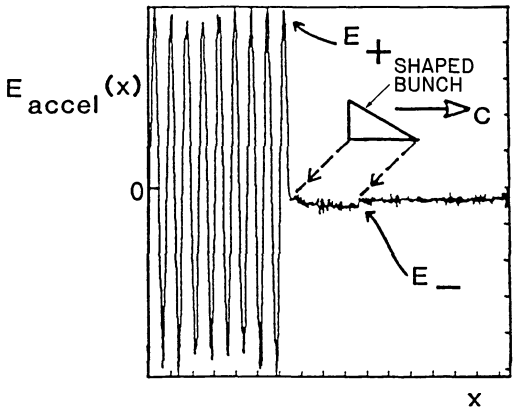

Figure 1 Computer simulation illustrating drive beam current and plasma electric field response in the plasma wakefield accelerator concept.

($\frac{\partial \vec{v}}{\partial t} = -e\,\vec{E}/m + \vec{F}_p/m$, where $\vec{F}_p$ is the pondermotive force or radiation pressure given by $-\nabla e^2 E_o^2/4m\omega_o^2$, E_o is the amplitude of the laser pulse envelope and ω_o is the laser frequency) into the time derivative of the continuity equation ($\frac{\partial}{\partial t}\left[\frac{\partial n}{\partial t} + \nabla \cdot n\vec{v}\right] = 0$, where n is the electron plasma density).

Linearizing $n = n_o + n_1$ and assuming immobile ions (valid for times much shorter than an ion plasma period $\left(t << \tau \sim \sqrt{M_i/m_e}\ 10^{-4}\ (1cm^{-3}/n_o)^{-1/2}\right.$, where M_i is the ion mass$\left.\right)$ gives a simple harmonic oscillator equation for the plasma density response:

$$\frac{\partial^2 n_1}{\partial t^2} + \omega_p^2 n_1 = -\omega_p^2 n_b(z-ct,r) + \frac{n_o}{m}\nabla \cdot \vec{F}_p \qquad (1)$$

where n_b is the drive beam density and Gauss' law was used to replace $\nabla \cdot E$ with $-4\pi e(n_1 + n_b)$. The electric field response can be found from the density n_1 and the wave equation which for wake-like solutions $\left(\partial_z = 1/c\partial_t\right)$ takes the form $\left[\nabla_\perp^2 + \left(\omega_p^2/c^2\right)\right]\underline{E} = 4\pi e \nabla n_1$. The solution for the longitudinal wake $W_z = eE_z$ is

$$W_z = 2mc\omega_p \int_{\infty}^{\xi} d\xi' \cos k_p (\xi - \xi') \int_o^{2\pi} d\theta \int r'dr' n_b(r',\xi') K_o \left(k_p |\vec{r} - \vec{r}'|\right)$$

(2)

$$+ \frac{k_p}{2} \int_{\infty}^{\xi} d\xi' \bar{F}_p (\xi', r) \sin k_p (\xi - \xi')$$

where $\xi = z - ct$ and $k_p = \omega_p/c$.

The details of the integrations over the modified Bessel function K_o can be found in Refs. 17 and 18. The transverse wake $W_r = -e (E_r - B_\theta)$ follows from an integration of the Panofsky-Wenzel theorem:

$$\frac{\partial W_r}{\partial z} = \frac{\partial W_z}{\partial r}.$$

Equations (1) and (2) show how beam and laser wakes are similar and how they differ. The main differences arise form the divergence term on the right hand side of (1). The laser term depends on the gradients of its intensity profile while the particle beam term depends on the beam density. For particle beam drivers the radial profile of the density response follows the radial profile of the driving bunch, while the width of the electric field response is the larger of the beam radius and the plasma skin depth c/ω_p. For laser drivers, the radial profile of the longitudinal wake follows the radial profile of the laser intensity. The extra divergence factor in Eq. (1) also accounts for the difference in the optimal longitudinal shape for laser and beam drivers. From Eq. (1) it can be seen that exciting a large wake requires a drive beam whose longitudinal profile has some frequency content at ω_p. This can be accomplished by a single pulse of duration on the order of π/ω_p, a series of short pulses separated by $2\pi/\omega_p$ or a long pulse with a sharp rise or fall. Of these possibilities, the case of a slow rise and sharp fall (e.g., a triangular bunch profile) is of particular interest because it corresponds to a large wakefield transformer ratio -- that is the ratio R of the maximum energy gain of a trailing particle to the energy of a particle in the driving beam[13]. For triangular bunches of rise length l_b and fall length short compared to c/ω_p, $R = l_b\omega_p/2c$. Examples of wakefields calculated from Eq. (2) for various

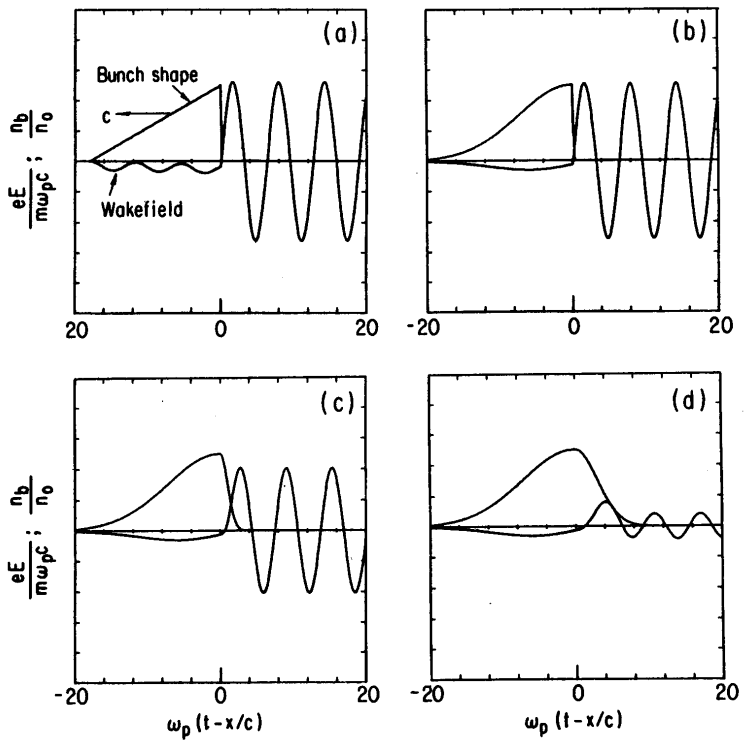

Figure 2 Numerical solutions of plasma wakes for various bunch shapes shown.

bunch shapes are shown in Figure 2. Figure 2 (d) shows how the wake is reduced if the bunch cutoff length is longer than c/ω_p.

For the experiment proposed here a large transformer ratio is not needed, so all that is required is a cutoff time that is short compared to $1/\omega_p$. We can accomplish this with a symmetric drive beam that is on the order of π/ω_p long. In Figure 6 we show the wake amplitude excited by the nearly symmetric SLC drive beam as a function of plasma density. This shows that there is an optimal plasma density for a given bunch length. The optimal density is a balance between the need for a density high enough to give a large wake and low enough to keep π/ω_p longer than the bunch length.

For $\sigma_r \approx 2c/\omega_p$, linear theory gives a wakefield amplitude of $W_z \approx 80$ MeV/m x $(N/10^{10})$ for a bi-Gaussian bunch of length $\sigma_z \sim .5$ mm in a plasma of density 2.5×10^{14} cm^{-3}. For smaller spot sizes, the wake increases approximately logarithmically[18, 19] as $1+ \log c/\omega_p\sigma_r$.

Although linear theory is strictly valid only for $n_b << n_o$, it is a useful guide (within a factor of two or so) even for very dense beams as long as the density that the beam would have at a spot size of c/ω_p is much less than the plasma density. This is

$$n_b \frac{\sigma_r^2}{c^2/\omega_p^2} << n_o \text{ or } Nr_e/\sigma_z << 1,$$

where r_e is the classical electron radius. This is a condition on beam current and corresponds to I << 2kA. For the proposed experiment $n_b/n_o \sim 10$, but $N r_e/\sigma_z \sim 0.2$. Thus we are near the limits of usefulness of linear theory.

B. The Non-Linear or Blowout Regime

For the case of dense ($n_b > n_o$), narrow ($\sigma_r < c/\omega_p$) beams the plasma response is highly non-linear and is dominated by the radial blow out[20] of all the plasma electrons within a radius $\sigma_r \sqrt{n_b/n_o}$. The plasma ions move relatively little on a short time scale, creating a uniform focusing force $F_r = 2\pi n_o e^2 r$ in the blowout region. A large longitudinal wakefield is possible when (after the passage of the beam) the ion space charge force pulls the electrons back, creating a large density spike on axis. The fields in front of the density spike have attractive properties for an accelerating structure. They provide linear focusing that is independent of z (i.e., $\partial W_r/\partial z = 0$) from which it follows that the accelerating field has a uniform profile (i.e., $\partial W_z/\partial r = 0$). For beam currents such that Nr_e/σ_z approaches one, the accelerating field is large (on the order of $\sqrt{n_o}$ V/cm). Although groups at UCLA, ANL and LBNL plan experiments to access the blowout regime, there has been no experimental test of this regime to date due to the relatively dense beams required.

The fully non-linear fluid equations for the plasma response to a beam are analytically tractable only in 1-D (valid for very wide beams). In 2-D the non-linear fluid equations in cylindrical geometry (r – z) have been solved numerically by B. Breizman in the simulation model Novocode.

The fluid description of a plasma breaks down if neighboring fluid elements cross. At this point, fluid quantities such as density become infinite. The crossing of fluid elements is associated with wavebreaking[21], a phenomenon that the fluid description is unable to model. Wavebreaking or fluid crossing is most severe at the point that the expelled plasma electrons return to and cross the axis. This limits the fluid models to mildly non-linear cases, or for the SLAC beam, to spot sizes larger than about 50μ. We will use the fluid models to quickly survey a large parameter space; however, to more accurately model the final parameters we will turn to particle-in-cell simulations. The PIC simulations use fully self-consistent 2-1/2D relativistic codes that are computer time intensive but have proven to be accurate models of experiments.

C. PIC Simulation Results

Sample results of a 2-1/2D PIC simulation in cylindrical geometry using the code MAGIC are shown in Figure 3. The parameters correspond to the expected experimental beam and plasma parameters described in the following sections. In Figure 3 the plasma density is 2.1 x 10^{14} cm^{-3} and the beam distribution corresponds to the 36 MV compressor setting described later. Figure 3a shows the real space of the plasma electrons in which blowout and crossing of streamlines are clearly visible. Figure 3b is a snapshot of the longitudinal wake 6 mm into the plasma. The peak accelerating field is 900 MeV/m. Figure 3c shows the axial current density J_z vs z. The beam's current profile and the plasma current (a large spike near the peak accelerating field) are clearly visible. Figure 4 shows simulations with parameters identical to Figure 3 but with a higher plasma density (n_0 = 9 x 10^{14} cm^{-3}). Here we see that the peak accelerating gradient is lower but, due to the shorter plasma wavelength, more particles in the tail experience a positive acceleration.

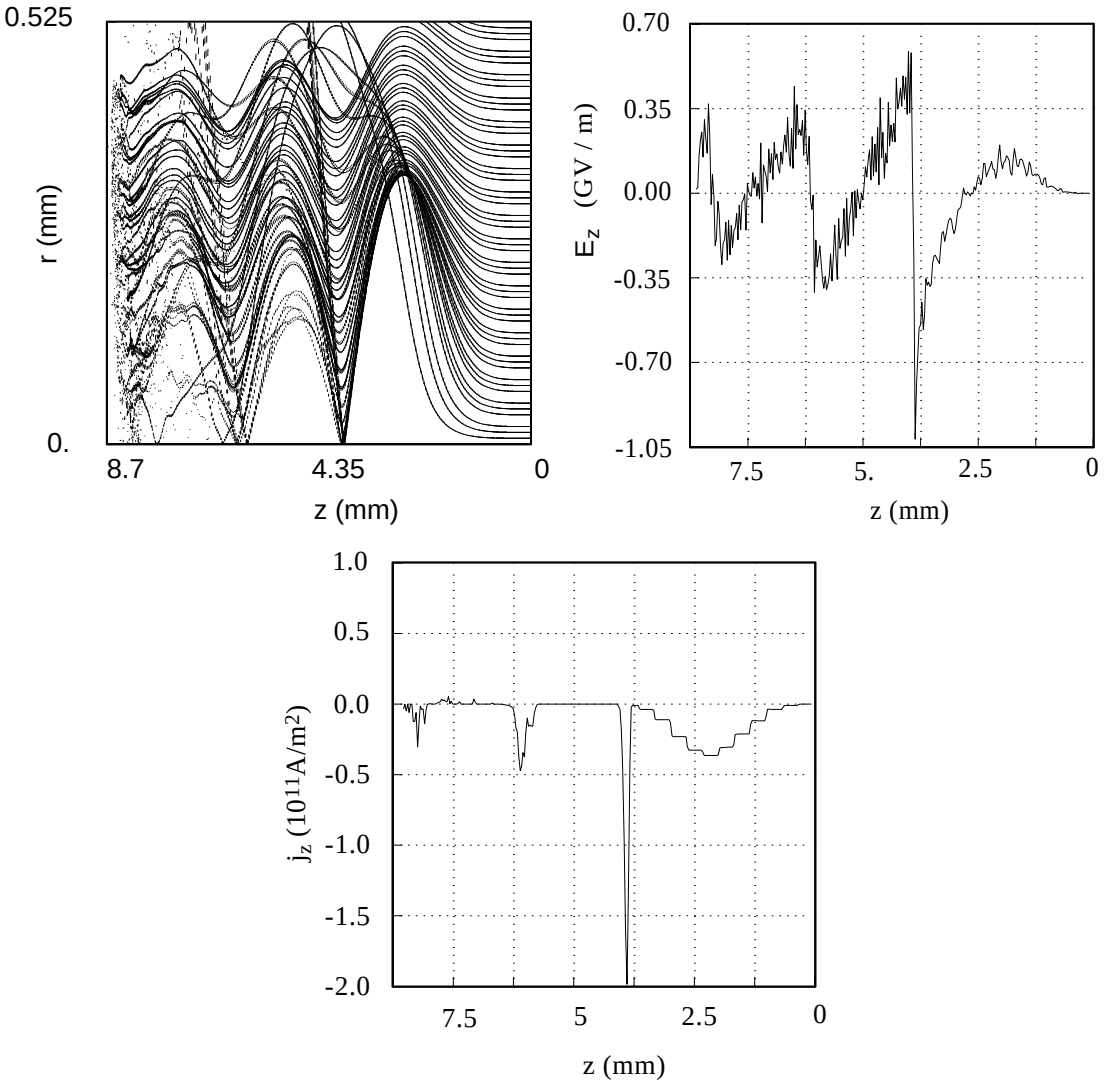

Figure 3 MAGIC PIC simulation of plasma wake for SLC beam (36 MV compressor setting) and plasma density 2.1 x 10^{14} cm^{-3}. (a) Real space r - z of plasma electrons; (b) axial electric field E_z; (c) axial current j_z.

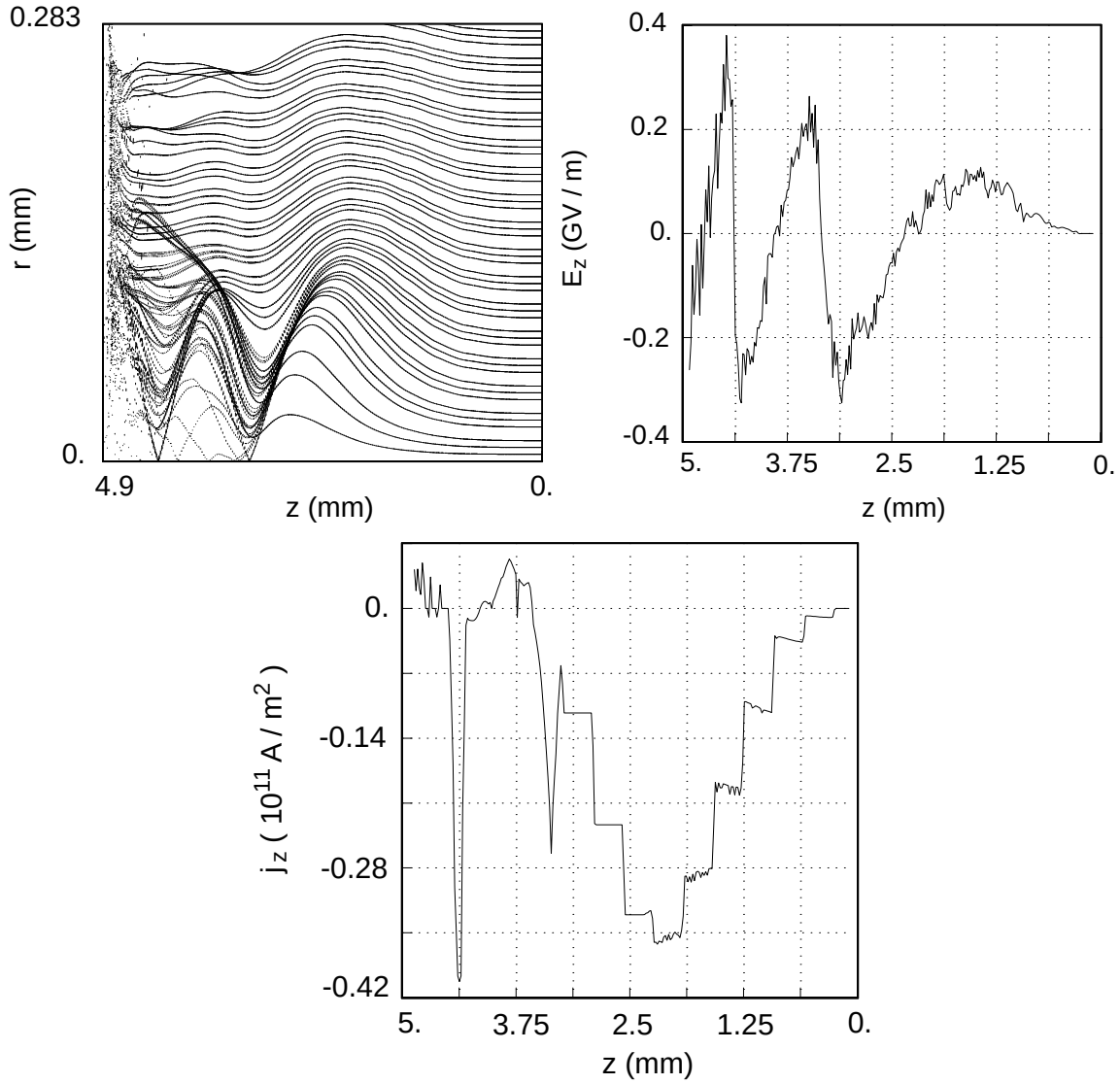

Figure 4 PIC simulation for a plasma density of 9 x 10^{14} cm^{-3}; all other parameters as in Figure 3.

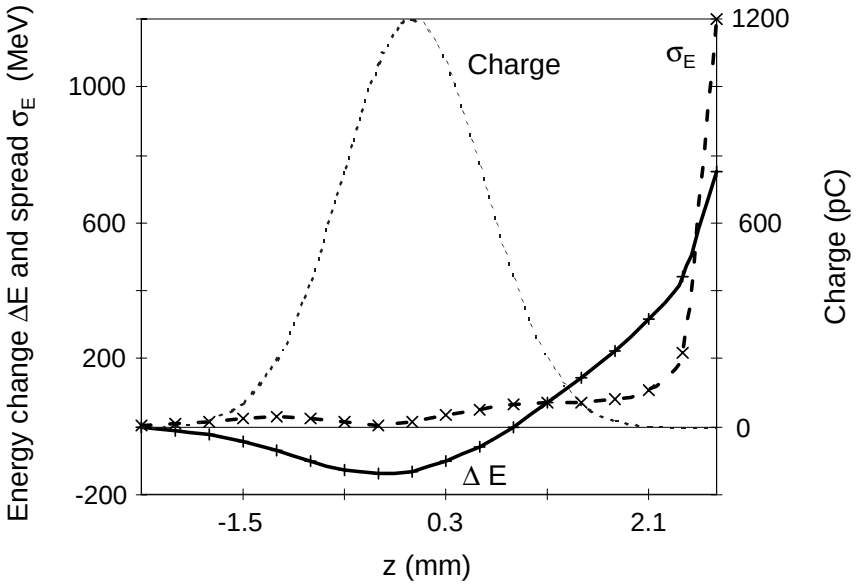

Figure 5 Simulated change of energy (solid line) and absolute energy spread (dashed line) of 1 ps slices along the bunch. This calculation was done for the same parameters as Figure 3 (plasma density of 2.1 x 10^{14} cm^{-3}). The two curves summarize the signature of plasma-wakefield acceleration as expected to be measured with the proposed diagnostic setup (compare Section V). The charge distribution is indicated by the dotted line.

In anticipation of the time-resolved diagnostic of energy change described in Section V, we simulate the experimental observables in Figure 5. Here we show the beam charge and the simulated beam energy change and beam energy spread in 1 ps intervals as they would be resolved with a streak camera. Even though some particles in the simulation gain over 1 GeV, the 1 ps window captures particles on either side of the acceleration peak. As a result, the energy change of the center of the last ps bin shown is roughly 800 MeV with a spread of 1200 MeV. Note that decelerating and accelerating fields within the bunch are well resolved with 1 ps diagnostic intervals.

To determine the optimal beam and plasma conditions for the experiment as well as to test the sensitivity of the experiment to variations in the plasma and beam parameters, we have performed a number of simulations similar to those in Figures 3 and 4. The results are summarized in Figures 6-9. Figure 6(a) shows the peak wake amplitude as a function of plasma density. The peak gradient is 900 MeV/m ± 100 MeV/m at a plasma density of 2.1 x 10^{14} cm^{-3}.

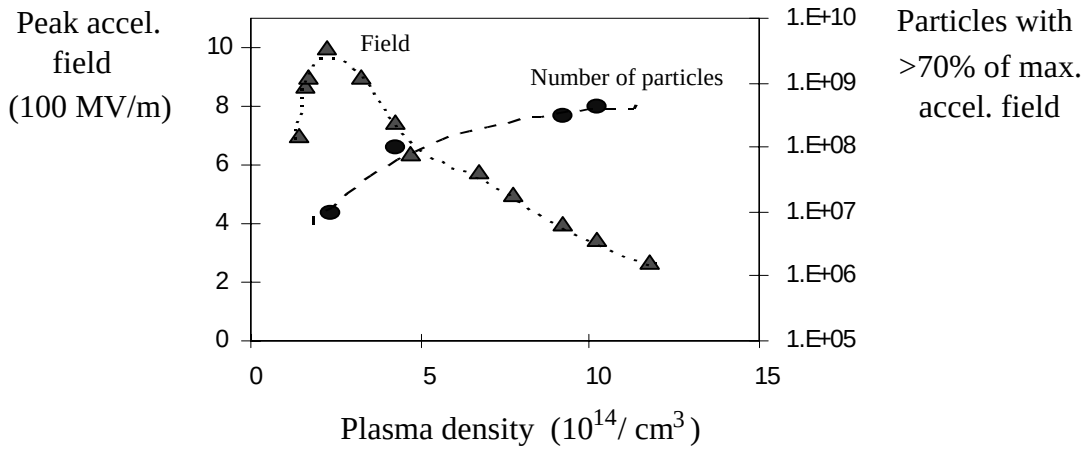

Figure 6 Peak wake amplitude vs. plasma density (36 MV compressor setting) and (dotted) number of particles experiencing 70% or more of the peak gradient.

The uncertainty quoted is due to numerical noise. As stated in Part A the peak corresponds approximately to a beam width matched to $\pi c/\omega_p$; at lower densities there is not enough plasma to support large wakes while at higher densities $\pi c/\omega_p$ becomes short compared to the bunch length. Also shown are the numbers of particles accelerated vs. plasma density. We comment that the wakefield response is very sensitive to bunch length. Shorter bunches give much larger gradients and correspond to higher optimal plasma densities. For example, for a Gaussian bunch with $\sigma_z \approx .4$ mm (about 60% of that in Figure 3), the peak gradient is 2.5 GeV/m at a density of 10^{15} cm^{-3}. Figure 7 shows the dependence of wake amplitude on number of beam particles. The amplitude scales nearly linearly in beam number. Figure 8 shows the sensitivity of wakefields to beam spot size. As expected, the wake amplitude changes very little with spot size for beam sizes much smaller than c/ω_p (≈ 375 μm for this density). Figure 9 shows the maximum wake amplitude that is achieved for each of the three compressor settings described in the next section. Clearly the 36 MV setting (i.e., the narrowest beam) is best.

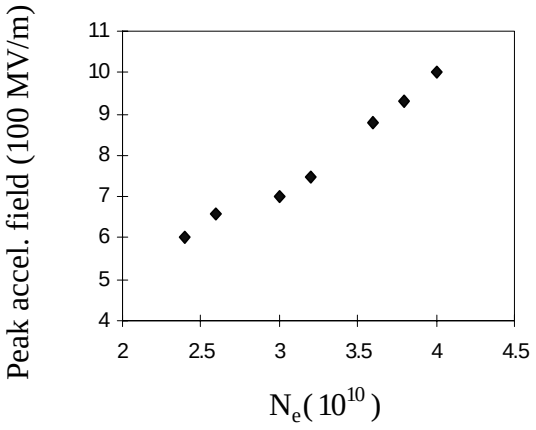

Figure 7 Wake amplitude vs. number of beam particles.

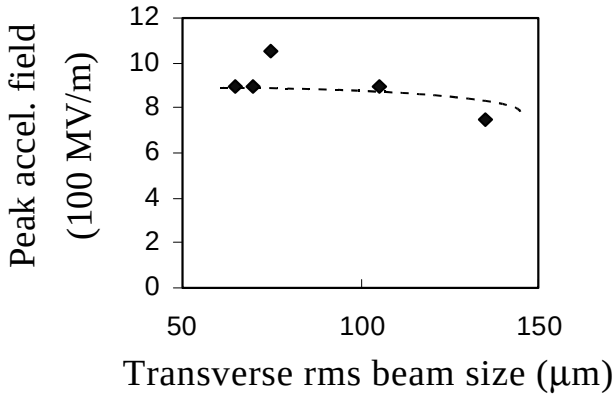

Figure 8 Wake amplitude vs. beam spot size (36 MV setting, $n_o = 2.1 \times 10^{14}$ cm^{-3}).

Since the plasma for the experiment will be produced by a laser of finite spot size, (see Sec. IV) we explored the effect of different plasma widths on wake production. For our nominal beam parameters we find that the wake amplitude begins to degrade for plasmas narrower than 300 μm in radius. This corresponds roughly to the maximum outward excursion one would calculate for the plasma electrons ejected by the beam. The dependence of wake amplitude on plasma radius is shown in Figure 10.

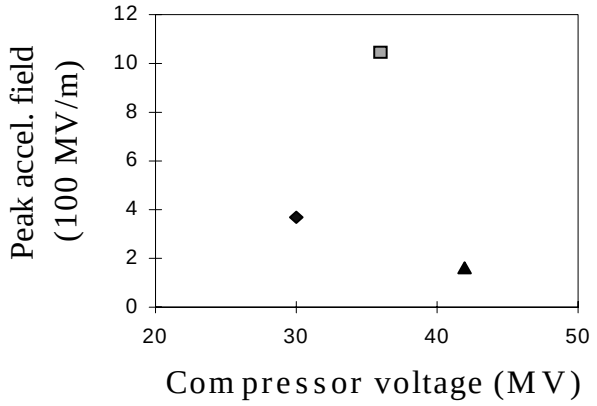

Figure 9 Peak wake amplitude vs. bunch compressor setting. Note that each point corresponds to a different optimized plasma density.

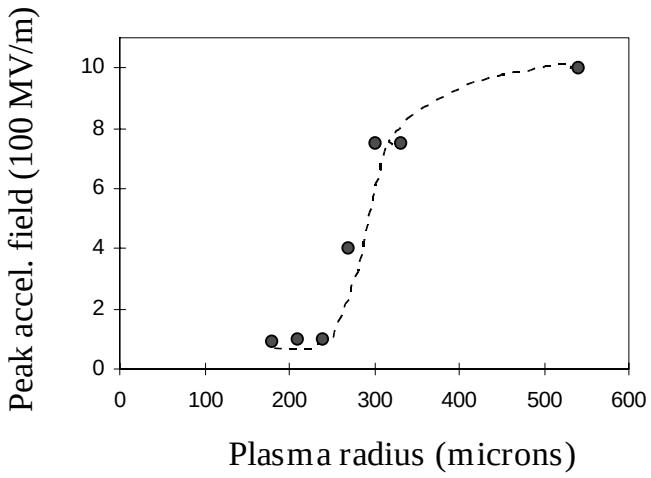

Figure 10 Wake amplitude vs. radius of plasma column.

One other consequence of a finite width plasma is the need for alignment of the beam and plasma axis. If the plasma is very narrow and the beam is off axis, the expulsion of plasma electrons by the beam will produce an ion column centered on the plasma axis which will deflect the beam. At the other extreme of a very wide plasma, the axis of the ion column is defined by the beam itself and no deflection of a collinear beam occurs. A transition between these two types of behavior occurs for our parameters and a beam jitter of ± 50 μm at a plasma radius of 250 μm. Thus a plasma of radius 300 μm or greater will simultaneously avoid wake degradation and beam deflection. If the beam has a head-tail offset, then the tail of the beam will be

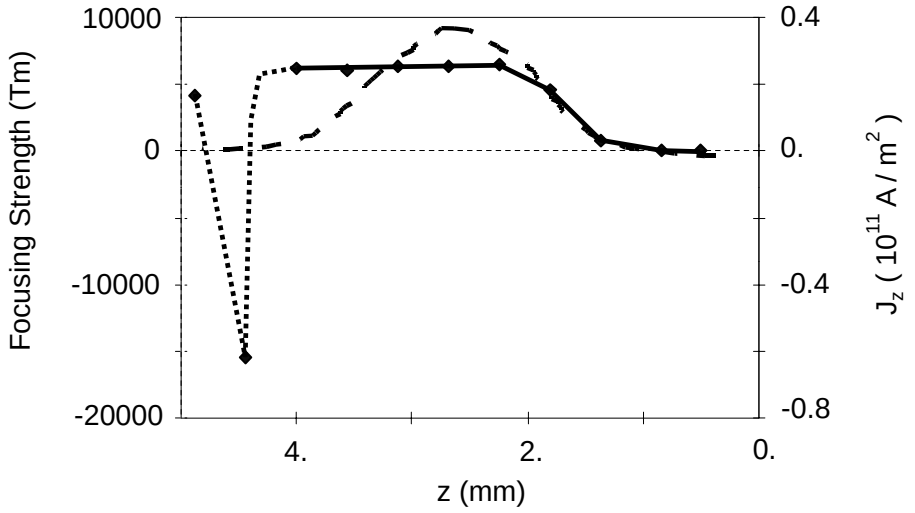

Figure 11 Focusing strength $-(E_r - B_\theta)/r$ (solid) and axial current J_z (dotted) vs. longitudinal position z for the PIC simulation of Figure 3. The points indicate the simulation results. Note that there is an important defocusing peak in the far tail of the bunch. Its width is unconstrained within the binning used for this simulation. However, it occurs only after the peak accelerating field. The axial current shows the longitudinal bunch distribution.

deflected toward and oscillate about the axis defined by the head. This leads to an angular deflection $\theta = k_\beta \delta \sin k_\beta L$ where $k_\beta \equiv \beta^{-1}$ is the betatron wave number described in the next section, δ is the offset of the tail and L is the plasma length. For typical $\delta = 25\mu m$ and $k_\beta \approx .08$ cm^{-1}, $k_\beta \delta = 2 \times 10^{-4}$ radians leading to a maximum 2mm offset 10m downstream. As described in Sec. III we will choose $k_\beta L$ close to $n\pi$ (n = 2, 4,…) to minimize this effect. For $k_\beta L$ exactly equal to a multiple of 2π the plasma is completely transparent to the beam with respect to its transverse dynamics.

D. Plasma Focusing Strength

As seen in the simulations in Figure 3a, the head of the drive beam rapidly blows out the plasma electrons leaving a positive ion column in the beam path. In this case, the transverse wake on the main body of the beam is particularly simple and takes the value given by a uniform

positive cylinder of charge density n_o: $W_r = 2\pi n_o e^2 r$. This corresponds to an effective quadrupole focusing strength (in both planes) of

$$W_r / r = 960\pi \text{ Tesla/m x } (n_o/10^{14}\text{cm}^{-3}) \quad (3)$$

The β-function for such a focusing channel is $\beta = \sqrt{2\gamma}\ c/\omega_p$, and the matched beam condition ($\beta = \sigma^2/\varepsilon$) occurs for an equilibrium radius of $(2\varepsilon_N^2/\gamma k_p^2)^{1/4}$. For our case, taking ε_N = 10 mm-mrad, $\gamma = 6 \times 10^4$ (30 GeV) and $n_o = 2.5 \times 10^{14}$ cm^{-3} gives $\sigma_{eq} = 4\mu$m and $\beta = 12$ cm.

Since the SLC beam will enter the plasma at a waist larger than this value, the spot size will over focus (plasma lens) at a point approximately $\pi\beta/2$ into the plasma. For a plasma density of 2.5×10^{14} cm^{-3} and a length L = 1.1 meters the beam would execute a total of three betatron oscillations.

The variation in the transverse focusing strength along the bunch in a PIC simulation is shown in Figure 11 (at $r = 1\sigma = 75\ \mu$m). From this we see the time-dependent focusing rising at the head then asymptoting to the theoretical value from Eq. (3) (6400 T/m for this case). The effect of the plasma focusing on the beam optics is discussed further in Sec. III.

III. Beam Delivery and Containment

Here we discuss the beam delivery and containment for the proposed PWFA experiment. Table 1 compares the beam parameters to be used in this proposal and the performance during SLC operation at 46.6 GeV. It is seen that the PWFA experiment could be done easily at 46.6 GeV. The assumed performance is well established from the SLC experience. However, in order to minimize the impact and cost of the proposed experiment, we plan for a 30 GeV experiment. PEPII will already accelerate beams up to 30 GeV. Due to requirements on the allowed energy spread (BNS) we will need 2 to 3 sectors of additional acceleration downstream of Sector 20. However, most of the RF in the last third of the linac needs not to be maintained and operated for the proposed experiment. Though planning for 30 GeV, it is important to note that the PWFA experiment can always be carried out at 46.6 GeV, if appropriate.

A. Interleaved Operation with PEPII

We propose that the PWFA experiment runs parasitically to the PEPII operation. Beam pulses not needed for PEPII injection will be transported into the FFTB experimental area at a rate of 10 Hz. This principle of interleaved operation for PEPII and SLC will be used extensively for the 1997/98 SLC run and the PEPII HER commissioning. We assume the same mode of operation and that necessary instrumentation remains operational after the end of SLC.

B. North Damping Ring and Bunch Compressor

The north damping ring must provide pulses of 3.5-4.0 10^{10} electrons at a rate of ~10 Hz. We further assume transverse emittances of ε_x = 30 mm-mrad and ε_y = 3.5 mm-mrad. These are standard SLC parameters. The use of the NRTL bunch compressor[22] is essential for the PWFA experiment. It must provide standard SLC performance and must be operated in a pulsed mode, as it was done in the past. Longitudinal bunch distributions for several compressor voltages have been measured in the SLC linac[23]. For this proposal we study three representative cases:

$$V_{compressor} = 30 / 36 / 42 \text{ MV}.$$

	PWFA	Standard SLC
Bunch intensity (*)	3.5-4.0 10^{10} electrons	3.5-4.0 10^{10} electrons
Bunch length (*)	0.6 mm	0.6-1.1 mm
Rate into the FFTB	10 Hz	1 - 120 Hz
$\gamma\varepsilon_x$ at LI02	-	30 mm-mrad
$\gamma\varepsilon_y$ at LI02	-	3.5 mm-mrad
Transv. rms jitter at LI30	< 50 μm	50% of spot size
$\gamma\varepsilon_x$ at IP-1	60 mm-mrad	45 mm-mrad
$\gamma\varepsilon_y$ at IP-1	15 mm-mrad	8 mm-mrad
σ_x at IP-1	< 100 μm	23 μm at 1.0 10^{10}
σ_y at IP-1	< 100 μm	37 μm at 1.0 10^{10}

Table 1 List of beam parameters for the PWFA experiment. The parameters are compared to the SLC standard performance at 46.6 GeV. The first two parameters (indicated by (*)) determine the plasma wakefield acceleration and are fundamental for the proposed experiment. Other parameters (the transverse beam emittances) are not critical for our experiment and can be worse.

The measured normalized bunch distributions are shown in Figure 12. The longitudinal bunch shape is preserved all the way into the FFTB. The compressor setting of 36 MV corresponds to full compression and provides the shortest bunch. Beyond that, the bunch length can be decreased by another 10-20% by so-called “bunch munching” (pre-compression in the damping ring). If one would like to go beyond that, an additional inexpensive bunch compressor could be built and installed at the beginning of the linac. This would not be compatible with parasitic running during PEPII operation. However, a second bunch compressor might allow for future extensions of this proposal, if the experiments show that shorter bunch lengths promise further progress.

C. SLAC Linac

The SLAC linac[24] will be in PEPII mode during our experiment. The RF downstream of the positron extraction point will be mostly switched off. We assume acceleration up to and including Sector LI20 is operational. The final beam energy at the end of the linac is then limited

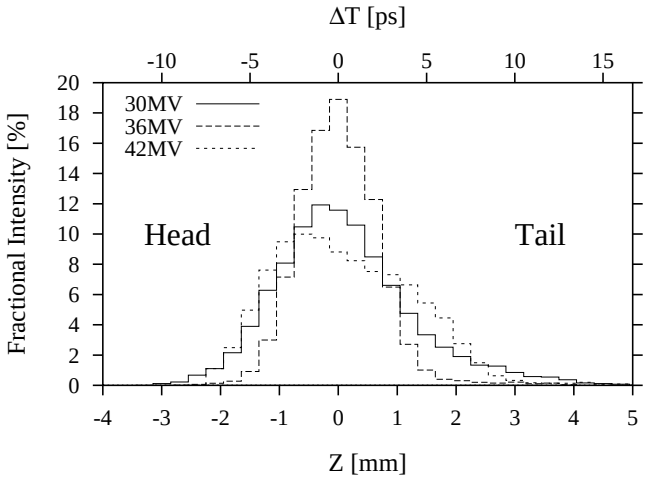

Figure 12 Measured longitudinal bunch distributions in the SLC. The distributions are normalized to an integral of one.

to about 30 GeV. However, it turns out that reasonable BNS damping will require additional acceleration in order to get to 30 GeV. If we do not compromise on the beam energy (constrained by the permanent magnets in the FFTB) we require about 2 to 3 sectors of acceleration after Sector 20. The locations of the additional sectors are not important and required power and maintenance costs would be minimal. In order not to restrict the location of additional RF, we assume in the following that we have no RF available for BNS damping after Sector 20 but more accelerating gradient up to there. Depending on the specific RF resources available during our experiment, a more realistic scheme will be prepared at the appropriate time. It is important to note that implementation of BNS is easier with additional acceleration downstream of Sector 20.

Because less magnetic field is required for the lower beam energy, the lattice can be scaled to the new energy without limitations from available quadrupole fields. We require that all quadrupoles, correctors and beam instrumentation in the last third of the linac remain operational after the end of the next SLC run.

The transverse beam dynamics in the linac[25] is more complicated at 30 GeV than at the nominal 46.6 GeV. It must be realized that the accelerating RF-voltage has two purposes in the linac:

1. Beam acceleration.
2. Manipulation of the correlated energy spread in the linac (implementation of BNS damping).

Having no RF available for BNS after Sector LI20 leaves no possibility to manipulate the correlated energy spread, while transverse and longitudinal wakefields do still apply in the last third of the linac. Because the relative energy spread into the FFTB should be small in order to avoid chromatic effects, there is a tradeoff between transverse emittance growth and jitter[26,27,28] on one hand and correlated energy spread on the other:

1. *Small correlated energy spread into the FFTB:* If the correlated energy spread for the FFTB is minimized, most of it is taken out by Sector LI20. After that the linac is operated with essentially no BNS damping. BNS damping in the rest of the linac is less efficient as well. Transverse wakefields cause emittance growth (beam breakup) and jitter amplification. The smallest correlated energy spread that can be achieved at 30 GeV is about 0.5% or 150 MeV absolute. The jitter would then be unacceptably large.
2. *Large correlated energy spread into the FFTB:* If the correlated energy spread is not taken out before the FFTB, then BNS damping can be significantly more efficient than in standard SLC operation. In this case the transverse emittances and the beam jitter would be better than for the 46.6 GeV SLC. However, the energy spread causes chromatic emittance growth in the FFTB, that must be kept reasonably small. The maximum correlated energy spread at the FFTB could be as high as 4%.

The tradeoff between those two extremes can always be changed during the PWFA experiment. For this proposal we have constrained the relative energy spread at the end of the linac to 1%. All the following simulations and calculations use this constraint. A suitable BNS setup was calculated for the 30 GeV operation of the SLAC linac and a short (fully-compressed) bunch. It turns out that RF-phases of 30 degree before and -45.5 degree after Sector LI08 constrain the final energy spread to 1%. The absolute beam energy and the relative energy spread in this case are shown in Figure 13 as calculated with the computer program LIAR[29,30].

As pointed out before, the large BNS phases cause a significant loss of acceleration. The average RF phase up to Sector 20 is then 40 degree. Let's consider the energy budget: The acceleration per linac sector is about 1.76 GeV on the crest. The maximum energy after

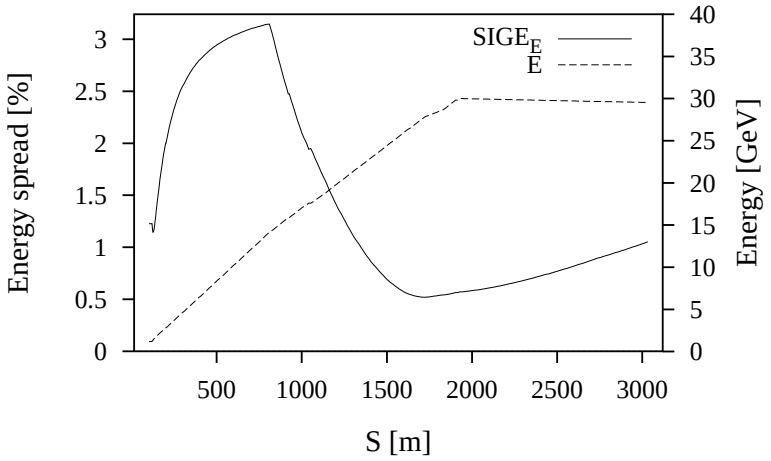

Figure 13 Simulated absolute beam energy and relative rms energy spread along the linac in PEPII mode of operation and with a fully compressed bunch (36 MV).

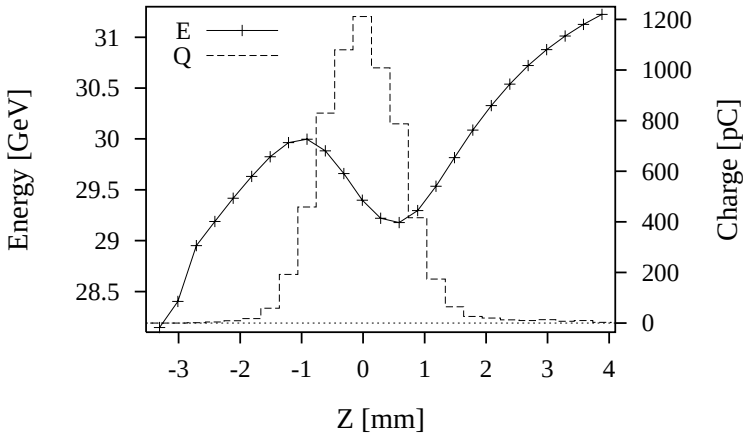

Figure 14 Simulated Energy-z correlation at the end of the SLC linac. The dashed curve shows the charge distribution within the bunch for a compressor setting of 36 MV.

19 sectors will be 33.4 GeV. Including the energy loss due to the large RF phases we can expect 25.6 GeV after Sector 20. Three sectors of acceleration on the crest will provide an additional 5.3 GeV which will bring the final energy to 30.9 GeV, leaving some headroom for broken klystrons. We see that in order to achieve a final beam energy of 30 GeV, additional acceleration from 2-3 sectors is required after Sector LI20. Due to short-range longitudinal wakefields and the curvature of the accelerating RF, the beam arrives at the FFTB with a significant correlation between beam energy E and longitudinal position *z* along a bunch. Figure 14 shows the simulated E-z correlation for the 1% final rms energy spread at the end of the linac.

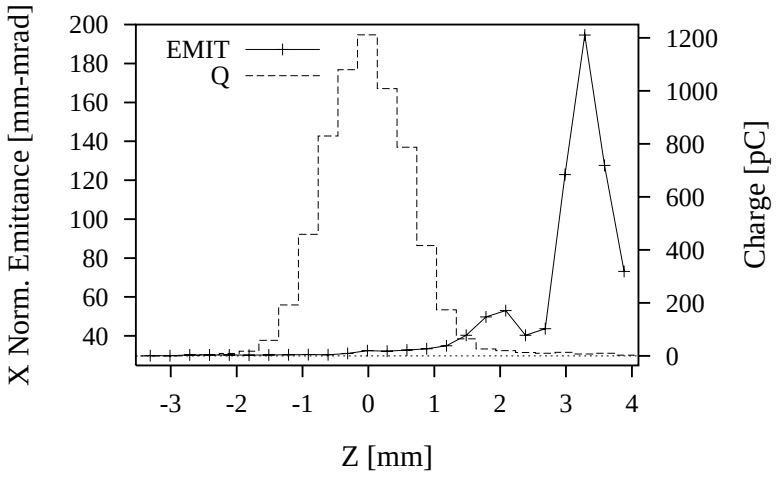

Figure 15 Simulated emittance of beam slices along the longitudinal direction z. The head of the bunch is at negative z. Tail slices show large chromatic emittance growth.

The beam sizes are not overly critical for the PWFA experiment. As discussed in Sec. II, the plasma wake is relatively insensitive to beam size for beams much narrower than $c/\omega_p \approx$ 150 μm - 350 μm. Thus we can accept emittance growth by more than an order of magnitude without jeopardizing the plasma wake. However, a reasonably small emittance growth is desirable to prevent smearing of the final energy spread diagnostic. This is discussed in Section V. We expect to minimize the transverse emittances at the entrance to the FFTB with SLC type "emittance bumps". Beam tails can be large in the linac, especially for a fully compressed bunch. The chromatic blowup of the tail is shown in Figure 15. Due to beam loading, the initial tail in z is becoming an energy tail that causes chromatic emittance growth. Since the PWFA experiment is not background sensitive, we can use the linac collimators in Sector LI28 to collimate the beam if needed.

Finally we consider transverse beam jitter. Pulse-to-pulse jitter at the end of the linac typically amounts to about 50% of the beam size; this corresponds to about 30 μm. The amplitude of the beam jitter is a strong function of the BNS energy spread profile. The BNS that we propose for the PWFA experiment is roughly as efficient as the standard SLC BNS setup. This is illustrated in Figure 16. The amplitude of an incoming betatron oscillation is roughly preserved along the linac. Insufficient BNS damping would result in beam breakup, seen as a large growth in oscillation amplitude. We expect roughly SLC performance for the beam jitter.

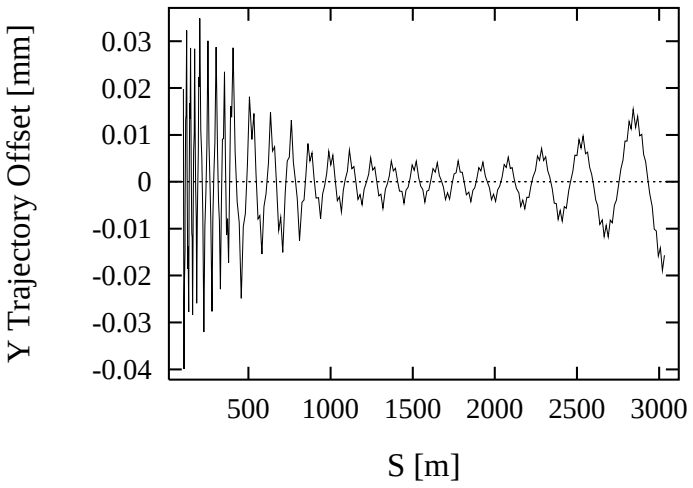

Figure 16 Simulated propagation of a vertical betatron oscillation along the SLAC linac. The oscillation amplitude is not growing resonantly. This illustrates that the calculated RF phases implement sufficient BNS damping. A horizontal betatron oscillation behaves similarly.

For 30 μm spot size at IP-1 we would therefore expect about 20 μm rms beam jitter. This is well below the requirement of 50 μm.

D. FFTB

The Plasma Wakefield Experiment will replace the E144 experimental apparatus at the IP-1 of the FFTB. There is plenty of space and the setup requires only minor modifications of the FFTB beamline. We have also considered the main focal point of the FFTB as a possible site. The available space at that location is, however, restricted to ~1 m, which is insufficient for our needs (~3 m).

The beam transport through the FFTB requires attention[31]. A few adjustments will allow for a 30 GeV beam in the FFTB while all safety requirements are fulfilled. An unavoidable beam mismatch at the plasma column causes beam blowup which must be kept within the diagnostics tolerances. From the linac we will enter the FFTB with a correlated energy spread of about 1% that must fit within the energy bandwidth of the FFTB.

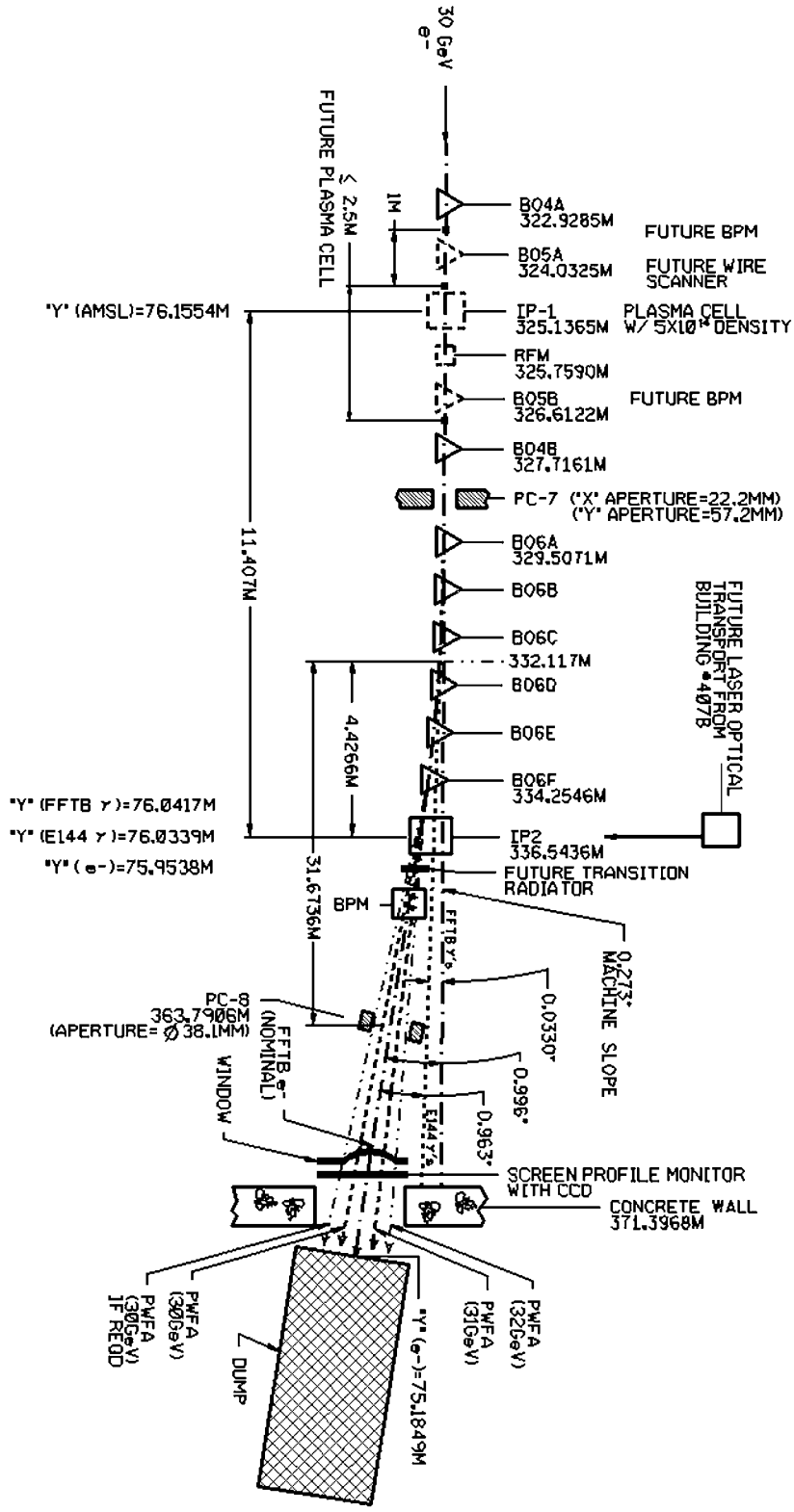

Figure 17 Layout of the Final Focus Test Beam (FFTB) area for the proposed plasma-wakefield acceleration experiment.

	ℓ_{eff} m	B kG	∫Bdl kG-m	ϕ degrees	ϕ radians	Gap mm
B04A, B04B	1	0.800	0.8	0.0295	5.147×10^{-4}	35
B05A, B05B	1	0.100	0.1	0.0037	6.43×10^{-5}	35
B06A—B06F	0.944	4.48	4.229	0.156	2.72×10^{-3}	38.1

Table 2 Summary of pertinent magnet data and the 46.6 GeV FFTB settings.

	Full Aperture		z-Location from STA100
	x	y	
PC-7	22.2 mm	57.2 mm	328.2 m
PC-8	38.1 mm diameter		363.8 m

Table 3 Apertures of collimators in the FFTB.

Layout of the FFTB Beam Line at 30 GeV

Figure 17 shows the layout of the FFTB for the proposed PWFA experiment. The important magnets and collimators are indicated. B04A and B04B are the "strong" soft bends, B05A and B05B are the "weak" soft bends. IP-1 and IP-2 are the E-144 (Nonlinear Compton Scattering Experiment) laser beam interaction points with the electron beam and the high-energy γ-beam, respectively. We propose to remove both the IP-1 target chamber and the "weak" soft bends B05A&B to make room for the plasma cell apparatus. The z-space thereby realized is ~3.5 m. B06A — B06F are permanent magnet dipoles (ALNICO-5) required as part of the beam containment system to safely deflect the electron beam onto the FFTB beam dump. PC-7 and PC-8 are fixed aperture, water-cooled copper protection collimators. They are full absorbers of the electromagnetic cascade shower which is generated when the electron beam is either mis-steered, or of the wrong energy and targets on them. They are part of the machine protection system, with the former protecting the vacuum chamber through the permanent magnet dipole

group, and the latter protecting beam diagnostic instrumentation and the penetration through the concrete shielding wall ahead of the beam dump.

The pertinent magnet data and 46.6 GeV FFTB settings are summarized in Table 2. Table 3 shows the apertures of the collimators. The total field integral of the six ALNIC0-5 dipoles is $\int$Bdl = 25.3747 kG-m which at an energy of 46.6 GeV deflects the electron beam by $0.93515° \equiv 16.326 \times 10^{-3}$ radians. Since this angle is fixed in order to reach the FFTB beam dump on the nominal trajectory, we need a smaller field integral for a 30 GeV PWFA experiment. It is cumbersome to degauss the magnets and then recharge them to the new total field integral required of $25.2747 \times 30/46.6 = 16.3357$ kG-m.

Consequently, we propose to completely discharge two of the magnets, B06A and B06F (in order not to change the common vertex of the array), and leave the four others as they are. This can be done *in situ* if we connect the charging coils to a portable power supply. However, as a consequence we can not remotely switch from 30 GeV to 46.6 GeV operation. The total field integral of the remaining four magnets is $\int$Bdl = 16.9165 kG-m which is $\Delta\int$Bdl = 0.5808 kG-m in excess of the required 16.3357 kG-m.

What is the "over-deflection" of a 30 GeV beam due to this field integral discrepancy? It can be shown that the effect of removing B05A&B is only $\Delta y \sim 1.4$ *mm* at IP-2 and $\Delta y \sim 4.8$ *mm* at PC-8. It can be fully compensated for by adjusting the excitation current of the remaining "strong" soft bends. Then we only need to consider the common vertex of the permanent magnet array and the appropriate drift distances to judge the effects of field integral and beam energy discrepancies. At 30 GeV, the field integral difference of 0.5808 kG-m results in a deflection angle difference of $0.03326° \equiv 0.5804 \times 10^{-3}$ radians. The drift distance from the common vertex to IP-2 is 4.427 m and the consequential "over-deflection" (downward) is $\Delta y \sim 2.57$ *mm*. Similarly, the drift distance to PC-8, the most important limiting aperture in that region, is 31.6736 m and the over-deflection is $31.6736 \times 0.5804 \times 10^{-3} = 0.01838$ m $\equiv 18.4$ *mm*. This would be just inside the aperture radius of 19.05 *mm*.

Now let's plasma wakefield accelerate the tail to 31 GeV. Where would such energies end up? Here we assume that the head and the tail of a bunch initially have equal energies. This

tends to overestimate the real plasma effect, since the plasma tends to compensate the initially correlated energy spread (compare Figure 14). The head initially has more energy than the tail, while the plasma decelerates the head and accelerates the tail. For a nominal deflection to the beam dump, we need $\int$Bdl = 16.8802 kG-m and we have 16.9165 kG-m. Then, $\Delta\int$Bdl = 0.03631 kG-m. So there will be an "over-deflection" downward of $\phi = 0.002012° \equiv 25 \times 10^{-6}$ radians. At IP-2, we find $\Delta y = 0.132$ *mm* and at PC-8, $\Delta y = 1.11$ *mm*. So, with no other field adjustments, the 31 GeV beam would very nearly follow the present nominal trajectory, but both the 30 and 31 GeV beams would be on trajectories which fall below the nominal trajectory. The difference between the two is $\Delta y_{30} - \Delta y_{31} \sim 17.3$ *mm*. Since any beam energy between 30 and 31 GeV is plausible, maybe even energies slightly above 31 GeV, and since the 30 GeV trajectory is relatively close to the limit of the PC-8 aperture, it might be prudent to place the two energy trajectories approximately equidistant from the center of the collimator aperture. The 31 GeV beam would then be ~9 *mm* above the center of the aperture and the 30 GeV beam ~9 *mm* below. This would leave ~10 *mm* clearance from the beams to the aperture.

Such trajectory adjustments can readily be made using B04A/B04B. What would it take to generate a 10 *mm* shift? If we use z = 325.3223 m as common vertex (near, but not at IP-1), then the distance to PC-8 is 38.5603 m and the deflection angle is 0.01489° ≡ 260 μradians. This would require a change of $\int$Bdl = 0.2688 kG-m total or 0.1344 kG-m per magnet. The magnets are now excited to generate $\int$Bdl = 0.8 kG-m. The reduction from 46.6 to 30 GeV would reduce this value to 0.515 kG-m. Since we need to raise the trajectories by ~10 *mm*, we just reduce B04A/B04B by $\int$Bdl = 0.1344 kG-m and operate them at $\int$Bdl ~0.381 kG-m.

Summarizing, the ray trace studies have shown that electron beam energies of both 30 and 31 GeV can be comfortably accommodated in the existing FFTB dump line downbeam of IP-1. To accomplish this, we propose that two of the six permanent dipole magnets are completely degaussed *in situ* with the four others remaining untouched. The two to be degaussed would have to be selected as a symmetric pair in order not to change the common vertex of the bend. Any pair will do, but intuitively we would pick B06A and B06F. The separation of the 30 and 31 GeV trajectories at IP-2 (a possible location for a detector) is $\Delta y \sim 2$ *mm* which should not present any hardship. Should we realize an energy gain in excess of 1 GeV, we could by further

adjustment of the excitation current of B04A/B04B accommodate as much as ΔE ~2 GeV at PC-8.

Note, we have assumed a monochromatic beam. The real beam will contain dispersive elements which can readily be scraped off by PC-8 should they be outside its acceptance aperture.

Radiation Safety and Beam Containment

Radiation safety and beam containment concerns in the context of the PWFA experiment only apply to the FFTB that will be operated with beam parameters that are significantly different from the FFTB standard values. All other beamlines and accelerators will be used with well established beam parameters.

The radiation protection systems for the FFTB[32], comprised of shielding and Beam Containment System (BCS), ensure safe operation of the beam line for the PWFA experiment. The BCS, a system which includes toroidal beam current monitors and ion chambers, limits the beam intensity, repetition rate and the amount of beam loss along the beam line. Currently, at 46.6 GeV, the FFTB BCS limits the average beam power to 2.3 kW and the beam loss to less than 1 Watt at any point. BCS also protects dumps and safety stoppers against excessive dissipation of beam power. All the FFTB dumps and stoppers can safely dissipate the high current beam operation. Thus, there are no new containment issues for the PWFA experiment at 46.6 GeV. With the degaussing of two of the safety magnets described in the previous section, the Beam Containment requirements will be met at 30 GeV as well.

Results of radiation surveys performed around the FFTB tunnel have established the largest measured radiation level to be 0.2 mrem/kW/h outside the shield that surrounds the FFTB dump. Using the beam parameters of 46.6 GeV, $4x10^{10}$ and 10 Hz, the largest radiation level outside the dump would be less than 0.6 mrem/h which is below 1 mrem/h, the design value for the shielding. At 30 GeV, for the same bunch intensity and repetition rate, the average beam power is even lower resulting in a dose rate of 0.4 mrem/h. Therefore, the radiation safety requirements for both 30 GeV and 46.6 GeV operations will be met. However, depending on the

nature of occupancy of the personnel working in buildings around the FFTB dump, and the operation schedule for the experiment, additional shielding may be added to the main FFTB dump. The need for added shielding or local shielding of experimental and diagnostic devices will be reviewed as part of safety approvals required for each experiment at SLAC.

Beam Spot Size at IP-1

The beam is transported to IP-1 and is focused there. The design rms spot sizes for E144 are 20μm in both transverse directions x and y. The beam sizes at IP-1 have been measured to be:

$$\sigma_x = 23\,\mu m \text{ and } \sigma_y = 37\,\mu m \quad (1\cdot 10^{10}\ e^-, 46.6\ GeV)\ .$$

This measurement was done for a beam energy of 46.6 GeV, an intensity of about $1\cdot 10^{10}$ electrons and normalized emittances of ε_x = 35 mm-mrad and ε_y = 4 mm-mrad. For high beam intensity wakefield effects in the linac will cause the normalized emittances to be significantly larger. As a conservative estimate we use normalized emittances of

$$\varepsilon_x = 60 \text{ mm-mrad and } \varepsilon_y = 15 \text{ mm-mrad}$$

at the end of the linac. The energy spread from the linac is assumed to be 1% rms. The expected beam sizes in the FFTB are calculated using third order beam transport. The FFTB magnet settings were modified in order to achieve minimal spot sizes at IP-1. Figure 18 shows the calculated horizontal and vertical spot size at the IP-1 focus point. It is seen that a round beam of about

$$40\ \mu m \times 40\ \mu m$$

is expected for IP-1. This is more than two times better than required. The calculated spot sizes include chromatic aberrations up to third order.

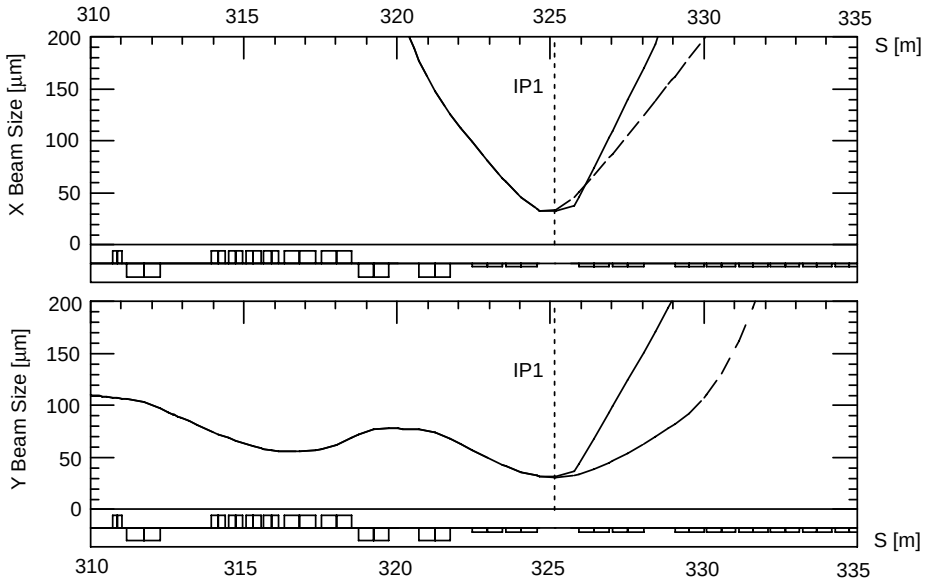

Figure 18 Spot sizes at the IP-1 location. The two curves were calculated with (solid line) and without (dashed line) a 1 m long plasma cell with 4000 T/m focusing strength.

Focusing Effect of the Plasma Column

The plasma column not only accelerates the beam but also acts as a plasma lens. The plasma can be described as a quadrupole that uniformly focuses in both planes. As discussed in Section II the beam will execute about three betatron oscillations in a plasma column of density 2×10^{14} cm^{-3} with a β-function of

$$\beta_x = \beta_y = 0.13 \text{ m}.$$

This must be compared to the projected β-functions at IP-1:

$$\beta_x = 1.1 \text{ m} \qquad \text{and} \qquad \beta_y = 1.7 \text{ m}.$$

The beam will experience a large beta mismatch that results in an emittance blow-up. Because we cannot match the beam into the plasma, the betatron oscillation in the plasma section

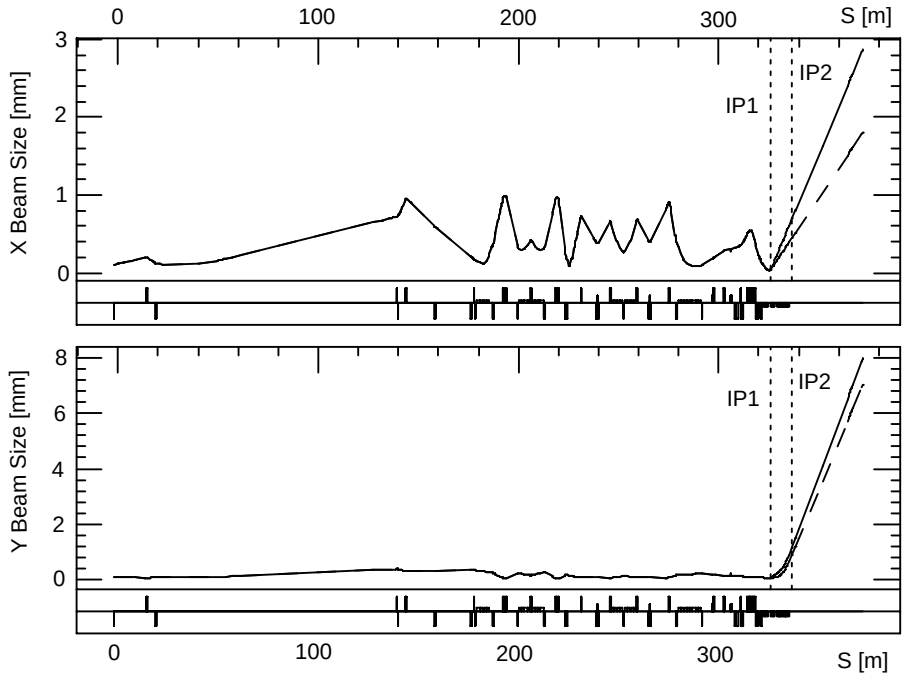

Figure 19 Simulated beam sizes in the FFTB with (solid line) and without (dashed line) a plasma lens of 4000 T/m ($n_0 = 1.4\times10^{14}$ cm^{-3}) at IP-1. The locations of IP-1 and IP-2 are indicated by vertical dashed lines.

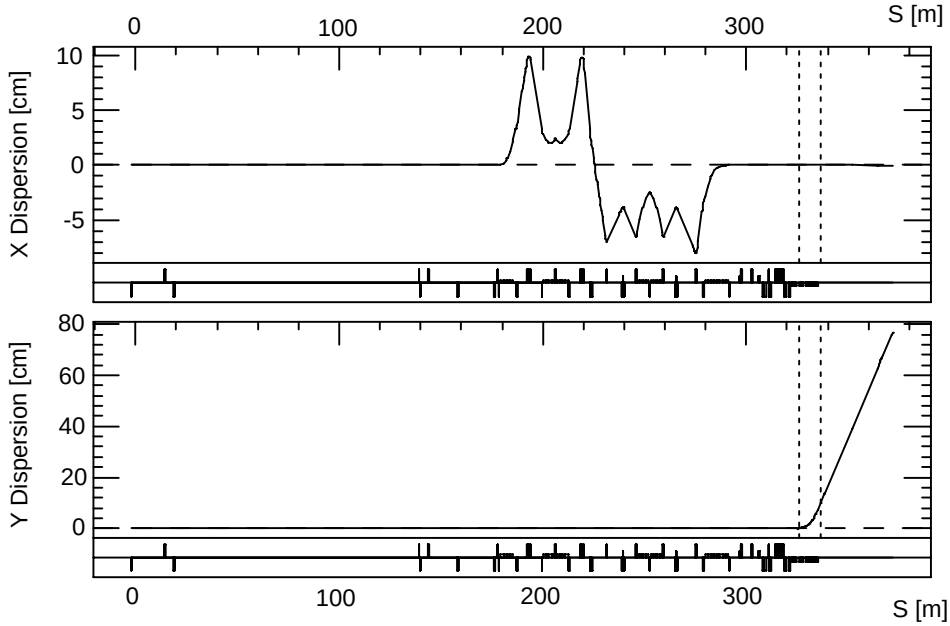

Figure 20 Design dispersion in the FFTB. The dashed vertical lines indicate the locations of IP-1 and IP-2.

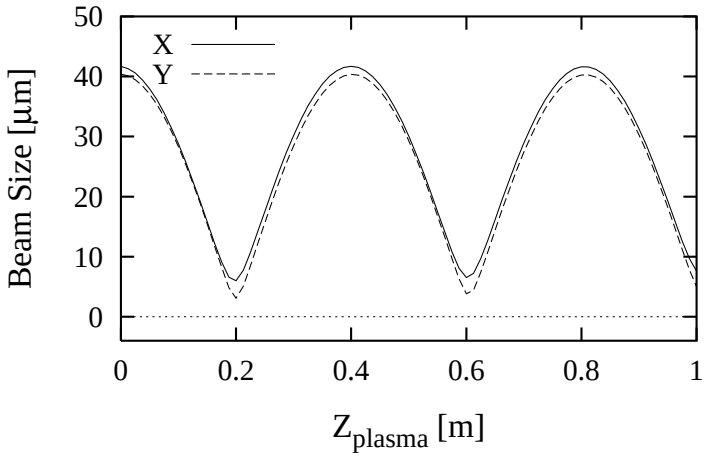

Figure 21 Horizontal (solid) and vertical (dashed) beam size within the 1 m long plasma cell and a plasma density of $n_0 = 2\times10^{14}$ cm^{-3} (solid line). The corresponding quadrupole strength is 6000 T/m.

(i.e., a thick lens) was included in the beam transport design. Figure 19 shows the rms beam sizes in the FFTB with and without a plasma column of 1.4×10^{14} cm^{-3} density. The sharp rise in spot size which can be seen is mainly due to the design of the dumpline. The plasma mismatch causes a change in beam size that is small compared to the design beam size. The design growth of the beam sizes is due to significant design dispersion after IP-1 and the end of the focusing lattice. The design dispersion is shown in Figure 20.

The mismatch effect from the plasma depends strongly on the phase advance inside the plasma column. Figure 21 shows the beam propagation for a plasma of $n_0 = 2\times10^{14}$ cm^{-3}. The corresponding quadrupole gradient is 6000 T/m. The horizontal and vertical beam sizes perform more than one betatron oscillation within the plasma. If the betatron phase advance within a plasma is a multiple of π, then the outgoing mismatch is minimized and the design beam sizes downstream are almost maintained. This is illustrated in Figure 22. The figure shows the spot sizes at the IP-2 location for different plasma densities (quadrupole gradients). Due to filamentation the mismatch effect increases with higher plasma density. However, local minima in beam size reflect the condition that the phase advance in the plasma cell is a multiple of π.

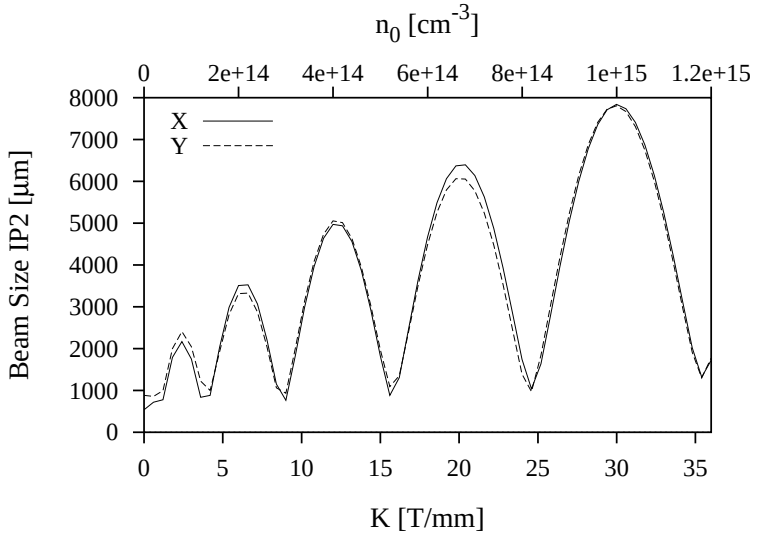

Figure 22 Horizontal and vertical beam size at IP-2 for different plasma focusing K (plasma density n_0). Several plasma densities allow the study of plasma wakefield acceleration while the downstream beam blowup is kept small. The calculation was done with a relative energy spread of 1%.

Dispersion Blowup

The diagnostics at IP-2 rely on a known vertical dispersion of about 100 mm. As a side effect from the betatron mismatch between beam and plasma any incoming dispersion can significantly blow up after IP-1. In simulations a 1 mm incoming vertical dispersion was found to be blown up by up to a factor of 100 with strong plasma focusing (30000 T/m at 10^{-15} cm^{-3} plasma density). Such a dispersion blowup could interfere with the time-resolved energy measurement. We therefore anticipate canceling any dispersion at IP-1 using dispersive bumps. The use of a wire scanner and high resolution Beam Position Monitors at IP-1 will allow very precise cancellation of dispersion.

Transverse Wakefield-like Deflections in the Plasma

The previous sections considered the focusing properties of the plasma cell. However, if the tail is offset with respect to the head of the bunch, then it will also be offset with respect to

the quadrupole center; the tail will experience a wakefield-like deflection. Because of the emittance growth in the linac, the beam will indeed have a “banana”-shape at IP-2. We can expect typical head to tail offsets of the order of tens of microns. A 25 μm offset of the tail can at worst generate centroid shifts at the transition radiator of about 2 mm. Though we could study and subtract this effect from our measurements, it would introduce an additional level of complication. Instead we adjust the plasma such that those wakefield-like deflections are largely avoided. As discussed in Section II C and shown in Figures 21 and 22 we accomplish this by adjusting the plasma density and length so that beam particles perform an integer number of betatron oscillations in the plasma column. If the phase advance in the plasma is a multiple of 2π, then the tail slice returns to its initial position and angle, independent of its offset with respect to the magnetic center of the plasma-quadrupole. The 1π phase advance condition is found by minimizing the transverse beam size of a 1 ps slice measured with a streak camera (compare Section V). From the plasma density it is then known whether the working point is at an odd or even multiple of π. The tail is either flipped in sign or should not have changed at all. This approach will work because the focusing along the plasma is expected to be rather uniform (compare Figure 11).

IV. Plasma Source

From the discussion in Sec. II, it is clear that this experiment requires a plasma source that is about 1 to 1.5 meters in length whose plasma density can be varied from 10^{14} to 10^{15} electrons per cm^3 and one that is quasi-uniform. The latter requirement can be somewhat quantified by assigning a density scale length $L = \{1/n_e(dn/dx)\}^{-1}$ where n_e is the mean electron density. For a linear density profile, $n_e(x) = n_o(1 + z/L)$, a 25% variation in density over 1 meter of length of the source will lead to a 12% variation in the wavelength of the plasma wave accelerating structure. This in turn will cause a phase slippage between the particles and the wave, which is quite acceptable. Thus, the density scale length should be greater than 4 meters. The next requirement is that the plasma source should be fully electron ionized so that any further electron impact ionization by the beam will not induce time-dependent variation in the plasma density in the frame of the electron beam. At the same time, there should not be a significant emittance increase of the electron beam due to collisions.

The ideal plasma source that fits all these requirements would be a fully ionized, meter long hydrogen plasma. However, hydrogen plasmas in this density range and of such lengths are very difficult to make. The same is true of a helium plasma. Furthermore, helium is difficult to pump and a sophisticated differential pumping system would have to be employed to guard against failure of any containment foil, especially if helium is being flowed through the plasma. We have therefore decided on a lithium plasma source that can simultaneously satisfy all the requirements on the range of required plasma densities, homogeneity, scalability (length), and that minimizes the problems of electron beam scattering and impact ionization.

Lithium, an alkali metal, is a solid at room temperature with extremely low vapor pressure. However, at 180°C it becomes a liquid and the vapor pressure of the liquid increases rapidly as the liquid approaches its boiling point of 1300°C. The required plasma densities between 2×10^{14} and 1×10^{15} cm^{-3} can be obtained by singly ionizing the lithium atoms (E_i = 5.9 eV). The vapor pressure required for this range of densities is 10 to 30 mTorr, which can be obtained at temperatures between 550 and 600°C, Such meter long lithium vapors have been produced at these and far higher (Torr-range) pressures in heat pipes for atomic physics and spectroscopy experiments.[33] In fact, a vast body of literature exists on producing sealed lithium

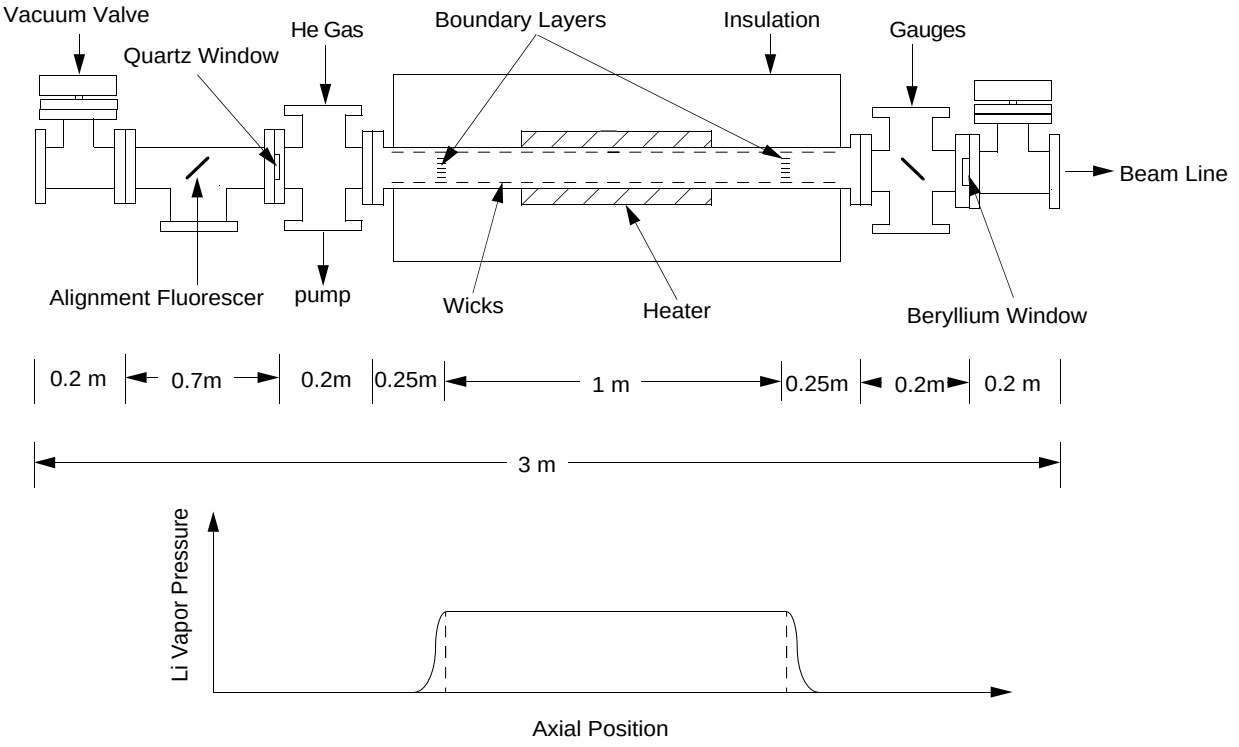

Figure 23 Schematic layout of the proposed lithium plasma source and its connection to the FFTB beamline.

heat pipes and producing and diagnosing lithium plasma using photoionization and spectroscopy/interferometry, respectively. After surveying the literature, we have designed such a source for our present application.

Figure 23 shows the schematic of the lithium plasma source. The first thing to note is that it is a completely sealed system with a few micron thick quartz window[34] on the upstream and a 25 μm thick beryllium window on the downstream end. Quartz was chosen because of its ability to transmit the 6 eV *photons* that are needed to photoionize the lithium vapor.[35] The second thing to note is that upstream of the source is a 1/2 meter ion tube with its own turbo-molecular vacuum system and a fast, feedback controlled vacuum valve that will isolate the FFTB beam line should the windows fail. In a lithium oven, the lithium vapor is confined in the heated region by a buffer gas, which in this case will be helium. Since the lithium can only exist as high pressure vapor in the heated region, pressure balance requires helium to move away into the colder region of the source. Thus, there is a boundary region where transition from mainly

lithium (on the hot side) to mainly helium (on the cold side) occurs. This boundary layer is typically 10 cm long[36], exists on both sides of the heated region and serves to confine the hot lithium vapor.

An advantage of this arrangement is that the lithium vapor is homogeneous and adjustable in length. Furthermore, the windows need not be heated making it very easy to make a vacuum seal. The 6 eV laser photon contained in an approximately 5 ns long, 25 mJ pulse are brought in from mirror box 3 (which is placed after the permanent magnets that are to be used to disperse the electron beam) placed approximately 11 meters from IP-1. The optical beam side is so arranged as to produce a focal spot radius w_o of about 300 μm (as discussed in Section II, see Figure 10). The Rayleigh range $2z_R$ to $2\pi w_o^2/\lambda$ of this beam is over 2.7 meters, so it will not spread appreciably over the length of the plasma column. The amount of laser energy needed to fully ionize the lithium vapor to Li^+ can be easily estimated. Since the ionization is a one photon ionization process, the laser energy needed simply depends on the ionization cross-section (σ_I) and the total number of atoms that are to be ionized. Taking $\sigma_I = 10^{-18}$ cm^{-2} at 6 eV, we estimate the total energy needed to be less than 5 mJ for the higher densities (10^{15} cm^{-3}) that are to be produced. Therefore, a laser pulse containing 25 mJ at 0.2 μm should be more than adequate.

Laser Source:

At present there are two options open. A frequency quintupled (x5) Nd:yag laser or an argon ion laser. Either would operate at 10 Hz and deliver about 25 mJ of photons at the final mirror box ready for insertion into the plasma source. The laser intensity is not an issue; only the laser energy as long as the laser energy is delivered in a time much shorter than the radiance and/or collisional recombination time of the lithium ion.[37] The next constraint is hydrodynamic expansion of the pencil-like plasma in the transverse direction. In the photoionization process, the electrons are born with the excess energy ($h\nu$ - 5.9 eV) leaving the ions essentially cold. The electron ion equilibration times[38] are on the order of 10^{-6} seconds, and in any event such an equilibrated plasma is so cold that transverse expansion of it may be neglected. Thus, a pulse of a few ns length will be perfectly suitable, making it possible to employ a simple stand-alone laser system in the same room as the FFTB BSM laser. As we understand it, the parts for the three mirror boxes which are needed to transport this beam from the laser area to the final mirror box

on the FFTB beam line are already on hand and machined. With laser pulses of a few ns length the timing between the laser and the electron beam becomes less of an issue than when synchronizing two ps long events. Further details on the construction and testing of this plasma source are described in Reference 39.

V. Diagnostics

The expected result of the Plasma Wakefield Acceleration Experiment is to observe deceleration and acceleration of up to 1 GeV within a single SLC bunch. The expected acceleration was discussed in Section II. Figure 5 shows the simulated changes in beam energy and energy spread due to PWFA for 1 ps slices along the expected SLC bunch. This energy change will overlay an incoming energy variation along the bunch (compare Section III). It is important to note that the incoming rms energy spread within a 1ps slice of the bunch will not exceed 100 MeV. From the expected plasma-induced energy change in Figure 5 we draw several conclusions:

1. The longitudinal charge distribution is roughly Gaussian with a sigma of 0.63 mm.
2. In order to diagnose the experimental results we need a time-resolved measurement of the energy along the bunch. This can be accomplished a streak camera.
3. A time resolution of 1 ps is sufficient to precisely analyze the plasma-generated beam deceleration and acceleration.
4. Considering particles up to 3σ into the tail we find an expected energy difference between the decelerated head and the accelerated tail of roughly 400 MeV. The 1 ps slice at 3σ in the tail shows an absolute acceleration of about 250 MeV.
5. The maximum slice acceleration is about 800 MeV with an induced energy spread of 1.2 GeV. The slice that experiences this maximum acceleration is about 4.5σ out in the tail of the particle distribution. Only very little beam charge can be observed there. From SLC measurements we expect to see about 10^7 particles (compare Figure 6).

It will be rather straight forward to measure plasma-induced energy changes within about 2.5σ of the particle distribution. Those measurements will test the plasma theory and simulation in detail. However, in order to diagnose the maximum acceleration we need to reliably measure charges down to 10^7 particles (or about 0.03 % of the total bunch charge) without worsening the time resolution of the streak camera. We will discuss the details of the streak camera measurements in subsection B. As mentioned in Section II we might also try shaping the longitudinal bunch distribution (known as “bunch munching” for SLC), such that the bunch gets shorter or such that we have more particles in the tail of the bunch. A shorter bunch will produce much higher

gradients (about 2.5 GeV/m for σ_z = 0.4 mm). More intensity in the tail will facilitate the streak camera measurement.

In the following subsections we describe the beamline diagnostics, the layout of the time-resolved energy measurement, and the plasma-diagnostics.

A. Beamline Diagnostics

A few additional diagnostic devices must be installed for a proper beam analysis. The intend is to put a wire scanner and a Beam Position Monitor (BPM) in front and immediately after the plasma cell in IP-1. We believe that the required hardware will be available after the end of the SLC operation. An existing Beam Position Monitor at IP-2 might need to be replaced with one of a larger aperture. The intended beamline diagnostic devices are indicated on Figure 17.

B. Time-resolved Energy Measurement

Basic Configuration: A transition radiator can be placed in the electron beam at a point near but downstream from IP-2. Transition radiation is produced at 45º, extracted from the vacuum through a quartz window and brought to an optical diagnostic station external to the radiation shielding. The light will be transported in a (low quality) vacuum. Remotely controlled mirrors for steering the light will be available. The optical diagnostic station will have the SLAC Hamamatsu N3373-02 streak camera as the primary detector. A streak camera trigger from the SLAC timing system will be available. Figure 17 indicates the proposed locations of diagnostic devices and the relevant distances.

Intrinsic Resolution: The SLC bunch length measurements shown in Figure 12 were done with the following parameters: slit width S = 100 μm, an optical interference filter centered at 500 nm with a 10 nm FWHM. The intrinsic resolution of the camera for SLC measurements was

$$\sigma^2(\mathrm{psec}) = 0.2772 + 4.52 \times 10^{-5} S^2(\mu\mathrm{m})$$

which leads to a resolution of σ = 0.85 psec = 0.26 mm.

Initial Light Intensity: We compare the expected intensity of the transition light to the synchrotron light intensity for the SLAC linac. For SLC measurements as shown in Figure 12 we observed synchrotron light over L ~ 1 m of path length for a ~ 47 GeV beam in an 11.9 kG field (ρ = 132 m, $\omega_c = 2.9\times10^{21}$ s^{-1}, $\omega/\omega_c = 1.3\times10^{-6}$). The energy radiated over a 10 nm bandwidth centered at 500 nm is

$$E_\gamma = \frac{L}{c} P(\omega)\omega\frac{\Delta\lambda}{\lambda} \approx \frac{1.3L}{c} P_\gamma\left(\omega/\omega_c\right)^{4/3}\frac{\Delta\lambda}{\lambda} = 1.45\times10^{-3}\text{eV}$$

This must be multiplied by the number of electrons to get the total radiated energy. The energy of transition radiation in the same bandwidth was calculated for $\gamma = 6\times10^4$ (30 GeV) to be

$$E_\gamma = \frac{dW}{d\omega}\Delta\omega = \frac{dW}{d\omega}\omega\frac{\Delta\lambda}{\lambda} = 1.2\times10^{-3}\text{ eV}.$$

This is comparable to the synchrotron light intensity that was used for the SLC measurements.

Chromatic Resolution and Available Light Intensity: The width of the optical interference filter at the streak camera determines chromatic effects on one side and the available light intensity for the streak camera on the other. This tradeoff is illustrated here:

Good resolution	$\Leftrightarrow$	High sensitivity
Small chromatic effects		High light intensity
Small filter width		Large filter width

The optimum filter choice will keep chromatic effects small enough so that the time resolution is not significantly worsened while the light intensity is maximized. The chromatic contribution to the resolution for SLC data has been measured to be ~ 3.7 psec for an optical filter with FWHM = 80 nm, so for FWHM = 10 nm, the chromatic contribution to the resolution would be ~ 0.47 psec. Because of this result a 10 nm filter width was used for SLC linac measurements with the

streak camera. The total resolution is σ = 1.0 psec = 0.33 mm. This is roughly 1/3 of the bunch RMS bunch lengths given in Figure 12. Resolution is adequate for the SLC bunch.

We tried to explain the measured chromatic contribution to the resolution with the amount of glass in the light path or path length effects. However, at this time we cannot explain the measured chromatic effect in the streak camera.

With a 10 nm optical interference filter charges down to a few 10^8 particles have been measured reliably at SLC. Note that measuring lower intensities was not important for SLC and therefore never tried. The experience at LBNL shows that smaller charges can be measured with good time resolution (however, with a different streak camera). In order to measure 10^7 particles with the SLAC streak camera the filter width would have to be opened by about a factor of ten, leading to 4 ps resolution if the chromatic effect cannot be corrected. At the present time we cannot decide whether it will be possible to open the filter width by a factor of ten while maintaining a time resolution of 1 ps. These effects will be studied further.

It is important to note, that even if we can not understand and avoid the chromatic contribution to the time resolution, we can still measure the tail of the beam with a larger time resolution. Measuring a 4 ps slice in the tail of the bunch, we would see a large energy spread of more than 1 GeV for this slice. Though not measuring the maximum acceleration as an acceleration of a single slice of the beam, we would still measure it directly through the energy spread.

Beam Optics: The streak camera will be set up to display time on one axis and vertical beam size and displacement on the other. The vertical dispersion D_y around IP-1 and IP-2 that is generated from the permanent magnets is shown in Figure 24. At IP-2 we expect a dispersion of about 100 mm.

A difference measurement will be made comparing beam pulses with plasma to those without plasma. The beam centroid will shift due to energy gain and dispersion. The dispersive centroid shift can be measured provided the change in spot size due to the mismatch introduced by the plasma is small compared to the centroid shift. Because the streak camera measures the

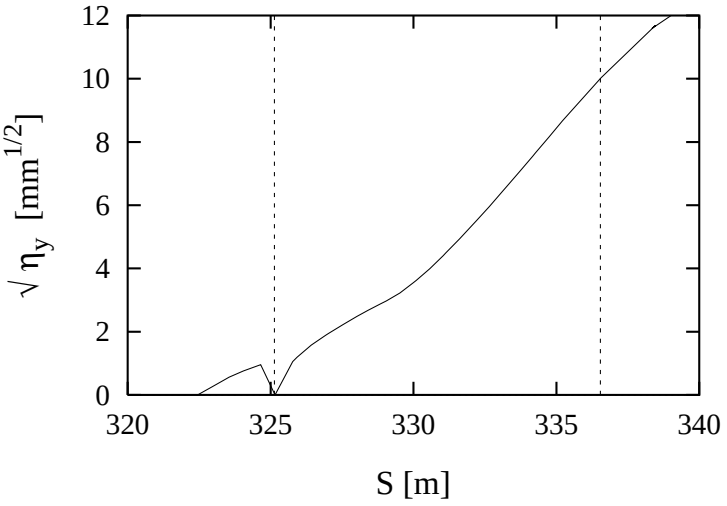

Figure 24 Vertical design dispersion in the region of the proposed PWFA experiment. The dispersion at the observation point IP-2 is expected to be about 100 mm.

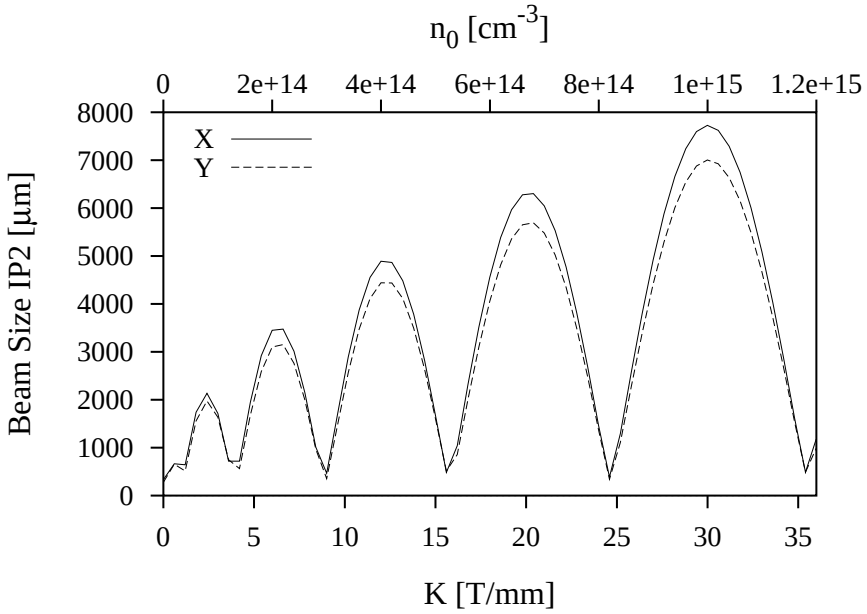

Figure 25 Calculated horizontal and vertical spot sizes at IP-2 *for a 1 ps slice* with 0.3% relative energy spread. The beam size is plotted as a function of plasma density.

beam in slices of 1 ps, the beam size for a single slice is calculated with a reduced energy spread of 0.3%. Figure 25 shows the expected spot size for 1 ps slice at IP-2 and as a function of the plasma density.

It is seen from Figure 25 that the spot sizes with and without the plasma cell are almost identical for certain plasma densities. The "transparency" condition for the plasma cell was discussed earlier. For minimum mismatch effects we expect a spot size for a single 1 ps slice of about 0.5 mm. This is comparable to the spot size of the whole bunch. The vertical deflection Δy due to an acceleration of 100 MeV is

$$\Delta y = D_y \frac{\Delta E}{E} = 0.33\,\mathrm{mm}$$

which should be easily measurable. The energy change between the decelerated head and the accelerated tail of the bunch is shown in Figure 5 to be about 400 MeV for particles within 2.5 sigma of the longitudinal distribution. It will be possible to measure the longitudinal wakefield along the bunch in detail. The maximum acceleration of 800 MeV for a 1 ps slice will show itself as a large offset (~2.5 mm) and a large vertical beam size (~4mm) due to the large induced energy spread (1.2 GeV). Generally the plasma-induced energy spread for a 1 ps slice is small (<80 MeV) and the vertical beam size is expected to increase by less than ~15%.

As discussed in Sections II and III, disturbing wakefield-like deflections might be caused by an offset of the beam tail in the head-induced focusing field. A 25 μm offset of the tail can at worst generate centroid shifts at the transition radiator of about 2 mm. This of course is undesirable, though we will measure the initial vertical slice offsets along the bunch and we could correct for that. However, we can largely avoid those wakefield-like deflections. Minimizing the spot size increase by betatron mismatch will allow to adjust the betatron phase advance in the plasma cell to a multiple of 2π. The plasma cell then is completely transparent.

C. Plasma Diagnostics

The experiment requires an online diagnostics of the plasma density-length product. The lithium plasma source will be well characterized by spectroscopic and interferometric techniques at UCLA and at SLAC before it is put into the FFTB beam line. Once on the FFTB beam line, the access to the source is rather limited to only the axial direction. The easiest way to monitor

the density is to measure the microwave radiation generated by the plasma in the 100 GHz to 300 GHz range after an electron bunch has passed through it, corresponding to a plasma density in the 10^{14}-10^{15} cm^{-3} range. This radiation is generated because the plasma rings at both the drivers' frequency ($\propto 1/\tau_{bunch}$) and the natural oscillation frequency (plasma frequency). The plasma frequency is proportional to $n^{1/2}$, the square root of the plasma density. The accuracy of this technique as an online diagnostic is limited to about 30% but will certainly tell us that the source is working and that the density is close to its pre-set value.

VI. Timetable

We are requesting three 3-week long blocks of beam time parasitic to PEP-II operation. In addition to this running time 3 weeks of setup time with unrestricted access to the experimental area is also needed. This time will be used to install and test the plasma source and diagnostics.

The run plan and goals for these three running blocks are summarized in the table below. The first block would be primarily used for setup and characterization, the second for parametric studies of plasma acceleration, and the third for continued parametric studies and for exploration of unanticipated phenomena.

Our proposal is that this work will be done parasitic to PEP-II operation as opposed to dedicated time. This mode of running should be established during the upcoming SLC/SLD run. There are two consequences of this. First, much like a test beam run, there will be low operating cost and few implications on scheduling of the linac. However, there is no experience with this type of operation at the present time, and we do not know what inefficiency to assign to performance of the experiment. For comparison we note that E144 had dedicated time with runs spanning 4 years and lasting typically 10 days. Their experience was that these running blocks were too short to respond to experimental problems and spaced so far apart that a significant amount of time was spent in setup of the FFTB at the beginning of each run.

Considering the positives and negatives of parasitic running and the E144 experience we are requesting three week long running blocks spaced within one 9 month PEP-II running cycle.

Block	Goals
1	Setup of beam, laser, plasma and diagnostic instruments Characterization of the beam and beamline optics with wire scanners and trajectory measurements Observation of acceleration with one set of beam optics, plasma density, and bunch length
2	Study of plasma acceleration versus i) plasma density and radius of the plasma channel ii) bunch length, beam intensity and beam optics
3	Continued study of parametric dependences Exploration of presently unanticipated phenomena

Table 4 Timetable for the proposed PWFA experiment. Each block of parasitic beam time covers three weeks. The three blocks should be spaced within one 9-month PEP-II running cycle.

[1] C. E. Clayton et al, K. Nakajima et al. To be published in Proc. Adv. Accelerator Concepts Workshop, Lake Tahoe, 1996 (AIP, NY 1997), S. Chattopadhay (Ed.).

[2] D. H. Whittum, W. H. Sharp, S. S. Yu, M. Lampe, and G. Joyce, *Phys. Rev. Lett.* **67** pp. 991-994, 1991; M. Lampe, G. Joyce, S. P. Slinker, and D. H. Whittum, *Phys. Fluids B* **5**, pp. 188-1901, 1993.

[3] V. E. Balakin et al, "Focusing of Submicron Beams for TeV-Scale E+ E- Linear Colliders", *Phys. Rev. Lett.* **74** pp. 2479-2482, 1995.

[4] M. Berndt et al, "Final Focus Test Beam: Project Design Report", SLAC-0376, Mar 1991.

[5] C. Bula et al (E144 Collaboration), "Observation of Nonlinear Effects in Compton Scattering", SLAC-PUB-7221, Feb 1996. Submitted to Phys. Rev. Lett.

[6] "PEP-2: An Asymmetric B-Factory." Conceptual design Report, SLAC-418, 1993.

[7] P. Chen, J. J. Su, J. M. Dawson, K. L. F. Bane and P. B. Wilson, "Energy Transfer in the Plasma Wakefield Accelerator", Phys. Rev. Lett. **56**, p. 1252, 1986.

[8] J. B. Rosenzweig et al, "Experimental Observation of Plasma Wakefield Acceleration", Phys. Rev. Lett. **61**, 98, 1988.

[9] G. Shvets and T. Katsouleas, private communication. The displacement of plasma electrons by the SLC beam increases the refractive index on the beam's axis and enables guiding of the laser light.

[10] J. Yoshii, C. H. Lai, T. Katsouleas, C. Joshi, W. B. Mori, "Cerenkov Radiation from Magnetized Plasma Wakes", submitted to Phys. Rev. Lett., 1997.

[11] P. Chen, J. M. Dawson, R. W. Huff, and T. Katsouleas, "Acceleration of electrons by the interaction of a bunched electron beam with a plasma," *Phys. Rev. Lett.* **54**, pp. 693-696, 1985.

[12] R. D. Ruth, A. W. Chao, P. L. Morton, and P. B. Wilson, "A plasma wakefield accelerator," *Particle Accelerators*, **17**, pp. 171-189, 1985.

[13] P. Chen, J. J. Su, J. M. Dawson, K. L. F. Bane, and P. B. Wilson, "Energy transfer in the plasma wakefield accelerator," *Phys. Rev. Lett.* **56**, pp. 1252-1255, 1986.

[14] T. Katsouleas, "Physical mechanisms in the plasma wakefield accelerator," Phys. Rev. A. **33**, pp. 2056-2064, 1986.

[15] R. Keinigs and M. E. Jones, "Two-dimensional dynamics of the plasma wakefield accelerator," *Phys. Fluids* **30**, pp. 252-263, 1987.

[16] For a detailed review of plasma acceleration, see E. Esarey, et al. "Overview of plasma-based accelerator concepts," *IEEE Trans. Plasma Sci.* **24** (2), 252 (1996).

[17] P. Chen, "A possible final focusing mechanism for linear colliders," *Particle Accelerators*, **20**, pp. 171-182, 1987.

[18] T. Katsouleas, S. Wilks, P. Chen, J. M. Dawson, and J. J. Su, "Beam loading in plasma accelerators," *Particle Accelerators* **22**, pp. 81-99, 1987.

[19] T. Katsouleas, J.J. Su, C. Joshi, W.B. Mori, J.M. Dawson, and S. Wilks: "A Compact 100 MeV Accelerator Based on Plasma Wakefields," SPIE Conf. Proc. OE/LASE '89; Los Angeles, CA (Jan. 16-20, 1989); p.428.

[20] J. B. Rosenzweig, B. Breizman, T. Katsouleas, and J. J. Su, Acceleration and focusing of electrons in two-dimensional nonlinear plasma wakefields," *Phys. Rev. A.* **44**, pp. R6189-R6192, 1991; D. Whittum, Ph.D. Thesis, UC Berkeley (1990).

[21] J. M. Dawson, "Nonlinear electron oscillations in a cold plasma," *Phys. Rev.* **133**, pp. 383-387, 1959.; T. Katsouleas and W. B. Mori, "Wave-breaking amplitude of relativistic oscillations in a thermal plasma," *Phys. Rev. Lett.* **61**, pp. 90-93, 1988; J. B. Rosenzweig, "Trapping, thermal effects, and wave wave breaking in the nonlinear plasma wakefield accelerator," *Phys. Rev. A.* **38**, pp. 3634-3642. 1988.

[22] R.L. Holtzapple et al., "Bunch Compression at the Stanford Linear Collider", SLAC-PUB-95-7014, Aug 1995. Presented at Micro Bunches: A Workshop on the Production, Measurement and Applications of Short Bunches of Electrons and Positrons in Linacs and Storage Rings, Upton, NY, 28-30 Sep.1995.

[23] R.L. Holtzapple, "Longitudinal Beam Dynamics at the Stanford Linear Collider", SLAC-Report-487. Ph.D. Thesis.

[24] J. Seeman et al, "The SLAC Linac as Used in the SLC Collider", SLAC-PUB-4890, Jun 1989. 4pp. Presented at 1989 IEEE Particle Accelerator Conf., Chicago, Ill., Mar 20-23, 1989. Published in IEEE Part. Accel. 1989 pp. 983-986.

[25] R. Assmann, "Beam Dynamics in the SLC". Invited talk at the PAC97, Vancouver. To be published.

[26] C. Adolphsen and Tim Slaton, "Beam Trajectory Jitter in the SLC Linac". SLAC-PUB-95-6905, May 1995. 3pp. 16th IEEE Particle Accelerator Conference (PAC 95) and International Conference on High Energy Accelerators, Dallas, Texas, 1-5 May 1995.

[27] R. Assmann and F. Zimmermann, "Possible Sources of Pulse to pulse Orbit Variation in the SLAC Linac", SLAC-PUB-7269, Aug. 1996. Talk given at 18th International Linac Conference (Linac 96), Geneva, Switzerland, 26-30 Aug 1996.

[28] F.J. Decker et al, "Higher Order Beam Jitter in the SLC Linac", SLAC-PUB-7260, Aug. 1996. Talk given at 18th International Linac Conference (Linac 96), Geneva, Switzerland, 26-30 Aug 1996.

[29] R. Assmann et al, "LIAR: A New Program for the Modelling and Simulation of Linear Accelerators with high Gradients and Small Emittances", SLAC-PUB-7300, Sep 1996. Talk given at 18th International Linac Conference (Linac 96), Geneva, Switzerland, 26-30 Aug 1996.

[30] R. Assmann et al, "LIAR - A Computer Program for Linear Accelerator Simulations" (Manual), SLAC/AP-103.

[31] P. G. Tenenbaum, "Expanded Studies of Linear Collider Final Focus Systems at the Final Focus Test Beam", UMI-96-21871-mc (microfiche), Dec 1995. Ph.D.Thesis.

[32] S.H. Rokni et al, "Radiation Protection Systems for the Final Focus Test Beam at SLAC", SLAC-PUB-6784-REV. Published in Health Phys.71:786-794,1996.

[33]C. R. Didul and F. B. Hulles, Rev. Sc. Inst., A2, 1779 (1971).

[34] W. Kimura, STI, private communication.

[35] Diamond Film reference.

[36] C. JR. Vidal and J. Cooper, J. Appl. Phys. 40, 3370 (1979).

[37] Ref. on recombination time of L^+.

[38] L. Spitzer, The Physics of Fully Ionized Gases.

[39] C. Joshi et al., A Meter Long Plasma Source for Advanced Accelerator Applications, to be presented at PAC 97, Vancouver.